Dalton Transactions

PAPER

Cite this: DOI: 10.1039/c6dt01409g

Dinuclear Au(I) N-heterocyclic carbene complexes derived from unsymmetrical azolium cyclophane salts: potential probes for live cell imaging applications†

Louise E. Wedlock,[a,b] Peter J. Barnard,[a,c] Aleksandra Filipovska,[a,d] Brian W. Skelton,[a,e] Susan J. Berners-Price*[a,b] and Murray V. Baker*[a,f]

Received 12th April 2016,
Accepted 3rd July 2016

DOI: 10.1039/c6dt01409g

www.rsc.org/dalton

We have synthesized a new series of azolium cyclophanes and used them as precursors of inherently luminescent dinuclear Au(I)–N-heterocyclic carbene (NHC) complexes. The azolium cyclophanes contained two azolium groups (either imidazolium or benzimidazolium), an *o*-xylyl group, and an alkyl linker chain (either C_2, C_3 or C_4). All of the azolium cyclophanes were characterised by X-ray diffraction studies and VT NMR studies, and all were fluxional in solution on the NMR timescale. The C_3- and C_4-linked azolium cyclophanes served as precursors of $Au_2L_2^{2+}$ complexes (L is a cyclophane bis(NHC) ligand). Due to the unsymmetrical nature of the azolium cyclophanes, the $Au_2L_2^{2+}$ complexes each existed as *cis* and *trans* isomers. X-ray diffraction studies showed that the $Au_2L_2^{2+}$ complexes had short intramolecular Au···Au distances, in the range 2.9–3.3 Å, suggestive of an aurophilic attraction, presumably as a consequence of the geometrical constraints imposed by the cyclophane bis(NHC) ligands. The complexes having the shortest Au···Au distances (*i.e.*, those based on C_3-linked cyclophanes) exhibited intense luminescence in solution. The uptake of one of the dinuclear Au–NHC complexes by tumorigenic cells, and its subsequent distribution and toxicity in the cells, was monitored by luminescence microscopy over 6 h and proliferation measurements, respectively.

Introduction

Cyclophanes have been of significant interest during the last decade, spurred on by studies into their interesting conformational behaviour,[1–6] their application for anion recognition,[4,7–10] and in the case of azolium cyclophanes, for their use as precursors to N-heterocyclic carbene (NHC) metal complexes.[5,11–21] In recent years there has been a high level of interest in the antitumour properties of Au(I)–NHC complexes.[22,23] In an early study in this area, we showed that some Au(I)–NHC complexes were toxic to tumour cells, but not to normal cells, and selectivity for tumour cells could be achieved by fine-tuning the hydrophilic/lipophilic balance through ligand design.[24] A mechanism of action involving selective inhibition of thioredoxin reductase (TrxR) in mitochondria of tumour cells has been proposed.[24,25] To this end, we have also reported a series of related lipophilic, cationic, dinuclear Au(I) complexes containing bridging bidentate NHC ligands derived from azolium-linked cyclophanes.[13,26,27]

Au(I)···Au(I) distances that are less than the sum of the van der Waals radii for the Au(I) ions are known to be weakly attractive, and such aurophilic interactions have been the subject of much attention in the scientific community.[28–32] Remarkable photophysical behaviour is often associated with compounds containing short Au(I)···Au(I) contacts,[33–38] a feature that has made them an important family of luminescent metal complexes, from both an experimental and theoretical perspective.[30,32] Previously, we have shown that for a family of dinuclear Au–NHC complexes where the NHC groups are part of a cyclophane framework, modification of the supporting cyclophane framework afforded control of the intramolecular

[a]School of Chemistry and Biochemistry M310, The University of Western Australia, Perth, WA 6009, Australia. E-mail: murray.baker@uwa.edu.au
[b]Institute for Glycomics, Griffith University, Gold Coast Campus, QLD 4222, Australia. E-mail: s.berners-price@griffith.edu.au
[c]Department of Chemistry, La Trobe Institute for Molecular Science, La Trobe University, Bundoora, VIC 3086, Australia
[d]Harry Perkins Institute of Medical Research, QEII Medical Centre, Nedlands, WA 6009, Australia
[e]Centre for Microscopy, Characterisation, and Analysis M310, The University of Western Australia, Perth, WA 6009, Australia
[f]Department of Chemistry, National Dong Hwa University, Shoufeng, Hualien 97401, Taiwan, ROC

†Electronic supplementary information (ESI) available. CCDC 834016–834025. For ESI and crystallographic data in CIF or other electronic format see DOI: 10.1039/c6dt01409g

Au···Au distance.[13,27] By carefully controlling this distance, the resulting luminescence excitation and emission maxima were fine-tuned to ranges suitable for mapping the distribution of the dinuclear Au–NHC complex inside living cells by luminescence microscopy, without the need for incorporation of an additional luminescent tag. In the present study, we have expanded on this theme and synthesized a series of unsymmetrical cyclophanes containing a single *o*-xylyl group, two azolium groups (either imidazolium or benzimidazolium), and a C_2, C_3, or C_4 alkyl linker, as potential precursors to dinuclear Au(I)–NHC complexes with short Au···Au contacts. Our purpose was to investigate the ability to control both the intramolecular Au···Au distance (to influence the luminescence) and the hydrophilic/lipophilic properties of the Au(I)–NHC complexes (to influence their sub-cellular distribution).

Results and discussion

Azolium salts

Synthesis and X-ray crystallography. Cyclophane salts **I**·2Br, **II**·2Br, **III**·2Br, **IV**·2Br and **V**·2Br were prepared by reaction of the appropriate bis(azole) with α,α′-dibromo-*o*-xylene under high dilution conditions (Scheme 1), and isolated by fractional crystallisation.

Crystals suitable for X-ray diffraction studies were obtained for each salt. The C_2- and C_3-linked cyclophane salts crystallised with water and/or solvent molecules (as **I**·2Br·2H_2O, **II**·2Br·(Me_2CO)·H_2O, and **IV**·2Br·EtOH), while the C_4-linked cyclophane salts **III**·2Br and **V**·2Br crystallised with no additional molecules. Structures of the cyclophane cations and associated bromide ions are shown in Fig. 1 and selected bond lengths and angles are summarized in Table 1, and unit cell contents are provided in the ESI (Fig. S1–S3†). The C_2- and C_3-linked cyclophane salts crystallised with molecules of water and/or solvent. Amongst the imidazolium-based cations, structures are seen where the imidazolium units are oriented in the same direction with respect to each other (*i.e.*, mutually *syn*, with the H2 hydrogens oriented away from the *o*-xylyl group; $\mathbf{II}^{2+}$), and in opposite directions (*i.e.*, mutually *anti*; $\mathbf{I}^{2+}$, $\mathbf{III}^{2+}$). Both of the benzimidazolium-based cations $\mathbf{IV}^{2+}$and $\mathbf{V}^{2+}$ adopt conformations in which the benzimidazolium units are mutually *syn*, with their H2 hydrogens directed beneath the *o*-xylyl moiety, presumably to avoid unfavourable steric interactions between the benzimidazolium C_6 ring and the *o*-xylyl moiety.[3,4] Interestingly, in all of the cations, the C_2, C_3, and C_4 linkers exist in staggered conformations. It may be that a preference for this type of conformation, avoiding unfavourable eclipsing interactions, is important in determining the relative orientation of the imidazolium groups in the macrocycles $\mathbf{I}^{2+}$, $\mathbf{II}^{2+}$ and $\mathbf{III}^{2+}$, in the absence of the type of steric interactions that favour the particular *syn* arrangement seen for the benzimidazolium groups in $\mathbf{IV}^{2+}$ and $\mathbf{V}^{2+}$.

In all cases, the close proximity of bromide counter ions to the H2 hydrogens of the azolium units is indicative of hydrogen bonding. For the C_2- and C_4-linked cyclophanes $\mathbf{I}^{2+}$, $\mathbf{III}^{2+}$ and $\mathbf{V}^{2+}$, each H2 hydrogen is associated with a different bromide ion (Br(1) or Br(2)). For the C_3-linked cyclophane $\mathbf{II}^{2+}$, in which mutually *syn* arrangement of the imidazolium groups dictates that the H2 hydrogens of the two azolium groups are close together (H···H ~ 2.69 Å; *cf.* H···H ~ 3.25 Å in $\mathbf{V}^{2+}$), both imidazolium H2 hydrogens are associated with the same bromide ion (Br(2)). In **I**·2Br·2H_2O, further hydrogen bonding is observed between Br(2), water molecules, and the non-cation bonded bromide ion, Br(1) (see ESI, Fig. S2†). The situation in the C_3-linked cyclophane $\mathbf{IV}^{2+}$ is more complex. In the crystal structure of **IV**·2Br·EtOH a single bromide counter ion was modelled as disordered over two sites, showing hydrogen bonding to the H2 hydrogens atoms of the cation (Fig. 1). The structure of the cation is significantly twisted (as is shown clearly in the diagram of the unit cell contents, ESI, Fig. S3†).

NMR spectroscopy. The ^{1}H NMR spectra of the *o*-xylyl linked cyclophanes suggested that in solution the cyclophanes adopted conformations similar to those seen in the solid state. In each case, however, the spectra were exchange-broadened in a manner consistent with processes involving interconversion between two equivalent conformations.

The ^{1}H NMR spectrum of a solution of the C_2-linked imidazolium cyclophane salt **I**·2Br in DMSO-d_6 at room temperature showed AA′XX′ patterns for the protons of the arene group (multiplets at δ 7.60–7 and δ 7.82–9) and ethylene group (apparent doublets at δ 4.22 and δ 4.77), a pair of doublets for the benzylic protons (δ 5.62 and δ 5.72) and apparent triplets for the imidazolium H4/H5 (δ 7.43 and δ 7.95) and H2 (δ 7.98) protons. The signal due to the imidazolium H2 protons is sur-

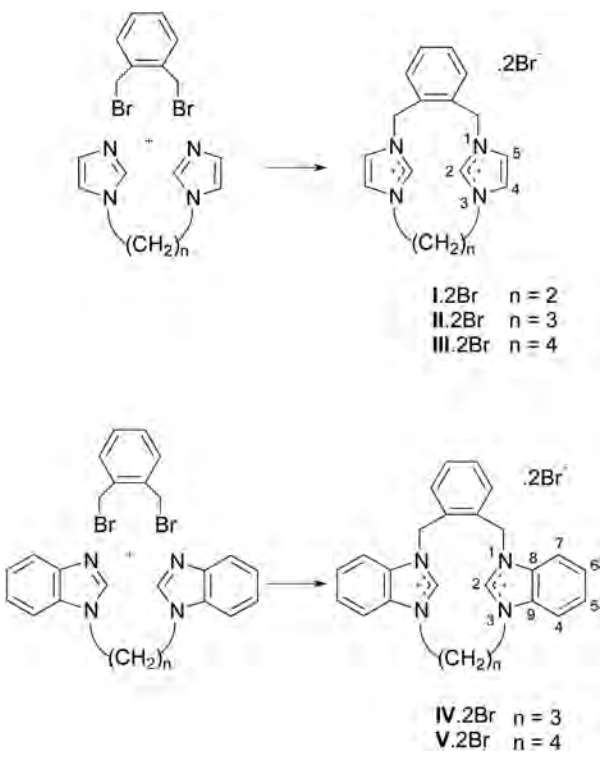

Scheme 1

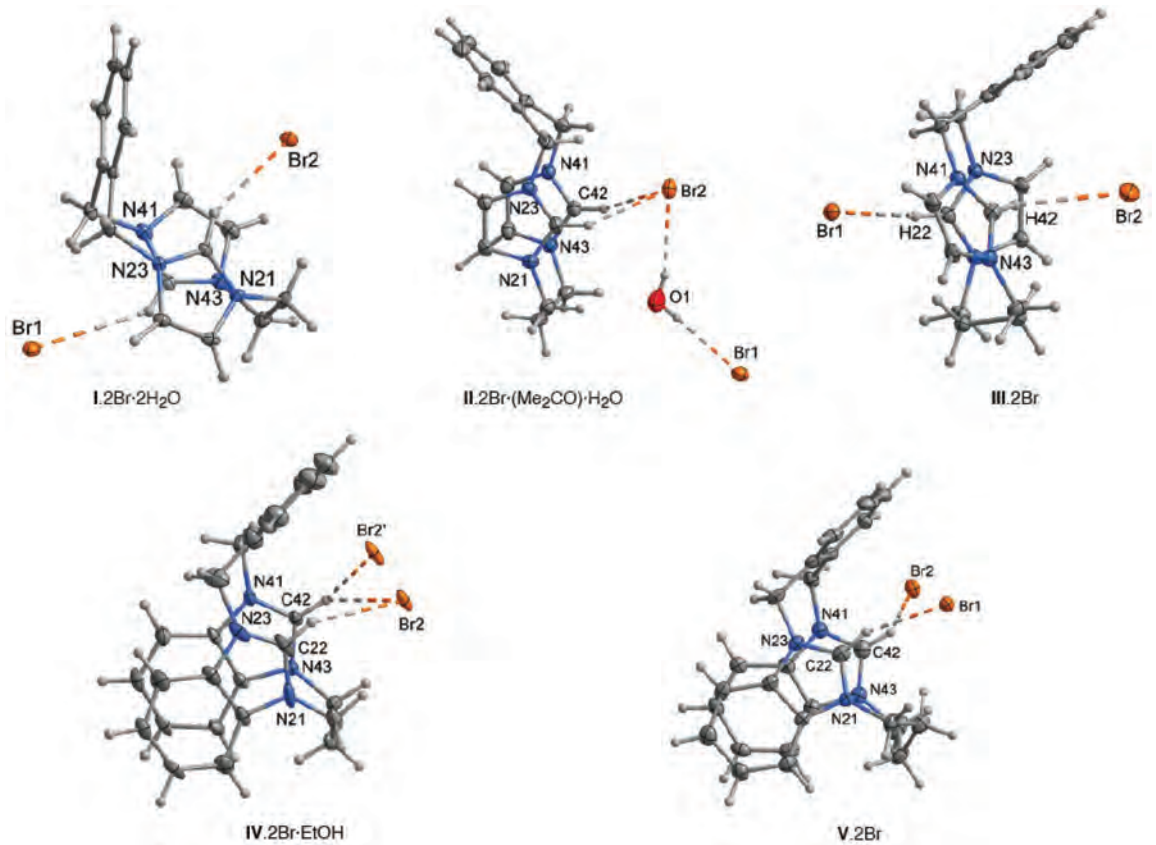

Fig. 1 Cations and associated bromide counter ions in the crystal structures of the azolium cyclophane compounds **I**·2Br·2H_2O, **II**·2Br·(Me_2CO)·H_2O, **III**·2Br, **IV**·2Br·(EtOH), and **V**·2Br, highlighting hydrogen bonding between the C2 hydrogens of the azolium units and the bromide ions. In the cation V^{2+}, the two C2′ atoms in the C_4 chain are disordered over two sites.

Table 1 Selected bond lengths and hydrogen bonding contacts for the asymmetrical azolium cyclophanes

	I·2Br·2H_2O	**II**·2Br·(Me_2CO)·H_2O	**III**·2Br	**IV**·2Br·EtOH	**V**·2Br
Space group	$P2_12_12_1$	$P\bar{1}$	$P2_1/c$	$P2_1/c$	$P2_1/n$
$N1_{21/41}$–$C2_{22/42}$ (Å)	1.346(3), 1.328(3)	1.330(4), 1.327(4)	1.332(3), 1.329(3)	1.348(12), 1.335(9)	1.349(6), 1.331(6)
$N3_{23/43}$–$C2_{22/42}$ (Å)	1.326(3), 1.346(3)	1.331(4), 1.327(4)	1.331(3), 1.341(3)	1.298(12), 1.346(9)	1.326(6), 1.337(6)
$H2_{22}$–$Br_{1/2}$ (Å)	2.60, 3.21	2.69, 2.81	2.52, 2.91	2.70, 2.55	2.67, 2.81
$H2_{42}$–$Br_{1/2}$ (Å)				2.74, 2.80	

prisingly upfield compared to the range of δ 8.5–9.5 typically seen for other imidazolium cyclophanes containing an *o*-xylyl linking group.[3,4] It may be that the H2 proton of each imidazolium group is magnetically shielded by the effects of the ring current from the other imidazolium group, and such shielding would seem likely if the conformation of $\mathbf{I}^{2+}$ seen in the solid state (Fig. 1) persists in solution.

Indeed, the number of ^{1}H NMR signals and their splitting patterns are consistent with the cyclophane $\mathbf{I}^{2+}$ existing in two equivalent conformations in which the imidazolium groups are mutually *anti* (as seen in the X-ray study) which interconvert by "flipping" of the xylyl group (Fig. 2a). An exchange process involving rotation of each of the imidazolium units about its N···N axis, but without flipping of the xylyl group, would also account for the appearance of the ^{1}H NMR spectrum. However, such an exchange process would seem unlikely to occur, given the small size of the cyclophane ring and the steric hindrance that would occur as the H2 or H4/H5 hydrogens "sweep" through the interior of the ring. The exchange process cannot involve both the flipping of the xylyl group *and* the rotation of the imidazolium groups, because that combination of processes would result in the signals due to the benzylic protons and the signals due to the ethylene protons both collapsing to singlets. The ^{1}H NMR spectrum of a solution of **I**·2Br in CD_3OD at room temperature (Fig. 2b) was similar to the one obtained in DMSO-d_6, except that the signal due to imidazolium H2 protons was absent (due to H/D exchange) and the benzylic protons appeared as an apparent singlet. As the temperature was lowered, the exchange process was slowed and signal broadening was evident (Fig. 2c and d).

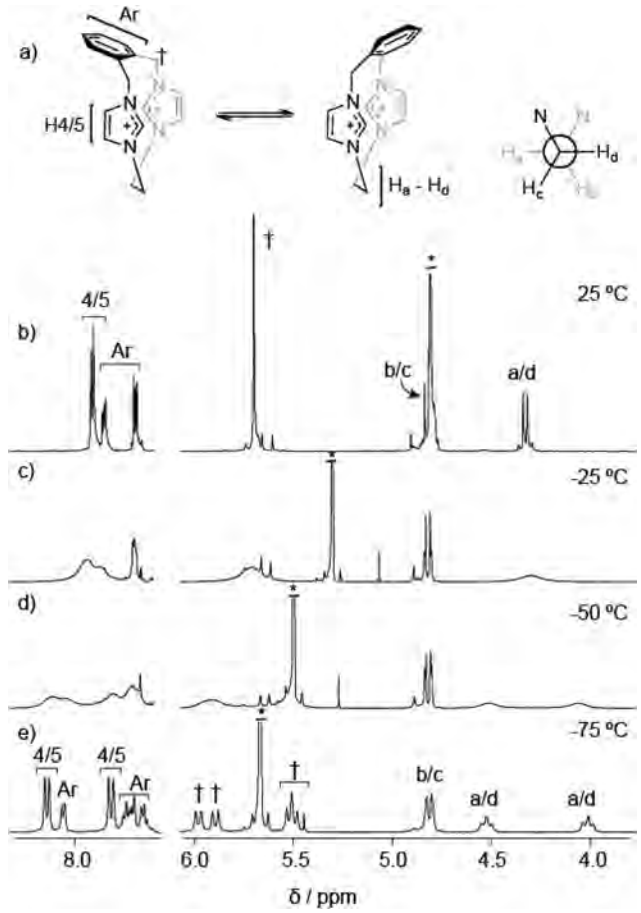

Fig. 2 Variable temperature ^{1}H NMR study of I·2Br. (a) Interconversion of equivalent conformations of $\mathbf{I}^{2+}$ by "flipping" of the xylyl group. (b)–(e) ^{1}H NMR spectra (500.1 MHz, CD_3OD) of I·2Br at 25, −25, −50, and −75 °C respectively. In (b), the signal due to H_b/H_c is partly obscured by the signal for adventitious water (labelled with an asterisk, *).

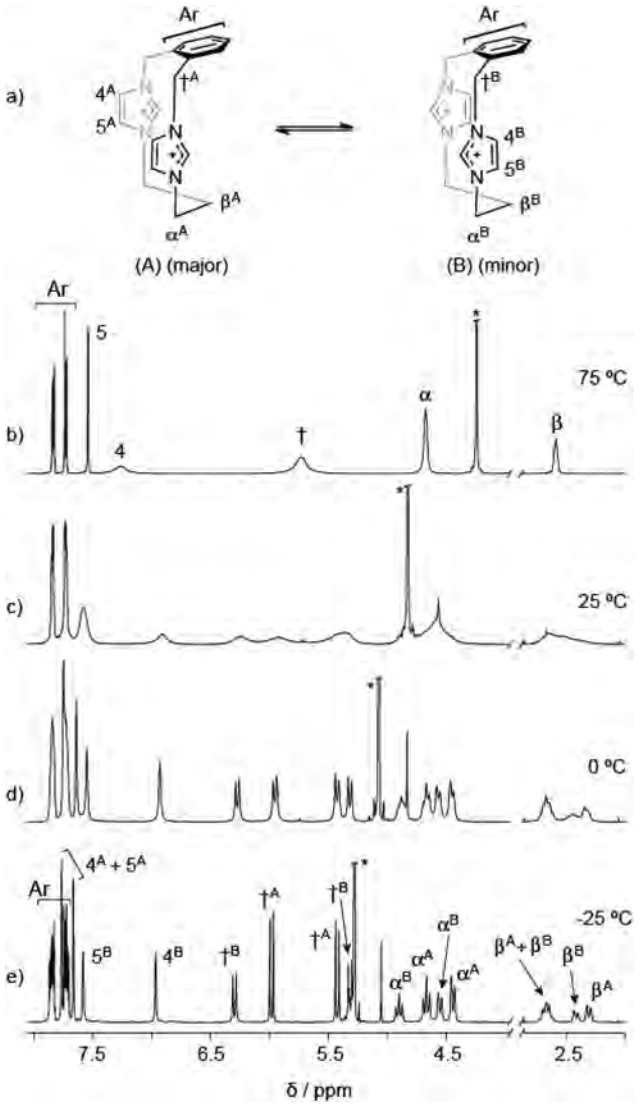

Fig. 3 Variable temperature ^{1}H NMR study of II·2Br. (a) Interconversion of the (A) and (B) conformations of $\mathbf{III}^{2+}$. The conformation of the C_3 chain could not be determined by ^{1}H NMR and for illustrative convenience is based on that seen in the X-ray study. (b)–(d) ^{1}H NMR spectra (500.1 MHz, CD_3OD) of III·2Br at 75, 50, and 25 °C respectively. The signal due to adventitious water is labelled with an asterisk, *).

At −78 °C (Fig. 2e), the spectrum showed a larger number of signals (*e.g.*, four doublets corresponding to four non-equivalent benzylic protons), consistent with the cyclophane $\mathbf{I}^{2+}$ being rigid on the NMR timescale, lacking any plane or axis of symmetry, in the conformation seen in the X-ray study. There was no evidence for the existence of a conformation of $\mathbf{I}^{2+}$ in which the imidazolium groups were mutually *syn*.

Fig. 3 shows the results of a variable-temperature ^{1}H NMR study of the imidazolium C_3-linked cyclophane **II**·2Br in CD_3OD solution. At room temperature (Fig. 3c), the ^{1}H NMR signals for the cation $\mathbf{II}^{2+}$ were broad, indicating that the cyclophane is conformationally labile on the NMR timescale. At higher temperature (Fig. 3b), various signals coalesce and sharpen (but most remain somewhat broadened), the number of signals being consistent with the cyclophane having an effective plane of symmetry that bisects the xylyl group and the C_3 chain. The broad signals seen at room temperature separate into signals due to two distinct conformations (A) and (B) (Fig. 3a) when the temperature is lowered (Fig. 3d) and the two conformations are eventually "frozen out" at −25 °C (Fig. 3e). The number of signals and coupling patterns for each of the conformations indicate that the imidazolium groups are mutually *syn* in both. For the major conformation (tentatively assigned as (A), Fig. 3a), the signals of the imidazolium H4 and H5 protons have similar downfield chemical shifts (δ 7.69 and 7.78). For the minor conformation (tentatively assigned as (B), Fig. 3a), the chemical shifts of the signals of the imidazolium H4 and H5 protons are quite different (δ 6.95 and 7.58), presumably because the H4 protons are magnetically shielded by the ring current associated with the xylyl group.[3] Interestingly, conformation (A) is intuitively the less sterically hindered of the two conformations, having the smaller portion of the imidazolium groups directed beneath the xylyl group,

but the intuitively more hindered (B) is seen in the solid state (Fig. 1). Perhaps in the solid state, H2···Br H-bonding tips the balance in favour of conformation (B), while in methanol solution, solvation disrupts the H2···Br interactions.[4]

Like its imidazolium analogue $\mathbf{II}^{2+}$, the benzimidazolium cyclophane $\mathbf{IV}^{2+}$ in solution exists in two conformations, but these conformations are rigid on the NMR timescale at room temperature. The ^{1}H NMR spectrum of a DMSO-d_6 solution of **IV**·2Br ([D_6]DMSO) at 25 °C (Fig. 4d and e) shows two sets of sharp multiplets, the number of signals, splitting patterns, and chemical shifts allowing the major and minor conformations to be assigned as (C) and (D) respectively (Fig. 4a). In this case, conformation (C) is strongly favoured over conformation (D), the latter presumably being destabilised by steric interactions between the xylyl group and the benzimidazolium groups. Due to magnetic shielding of the benzimidazolium H2 proton in conformation (C) by the ring current associated with the xylyl group,[3] the signal of this proton (δ 8.94) appears significantly upfield of the signal of the H2 proton for conformation (D) (δ 10.34). At elevated temperatures (Fig. 4b and c), ^{1}H NMR signals due to the minor conformation (D) broaden and merge into the baseline and signals due to the major conformation (C) also significantly broaden, suggesting that the two conformations interconvert on the NMR timescale at elevated temperatures.

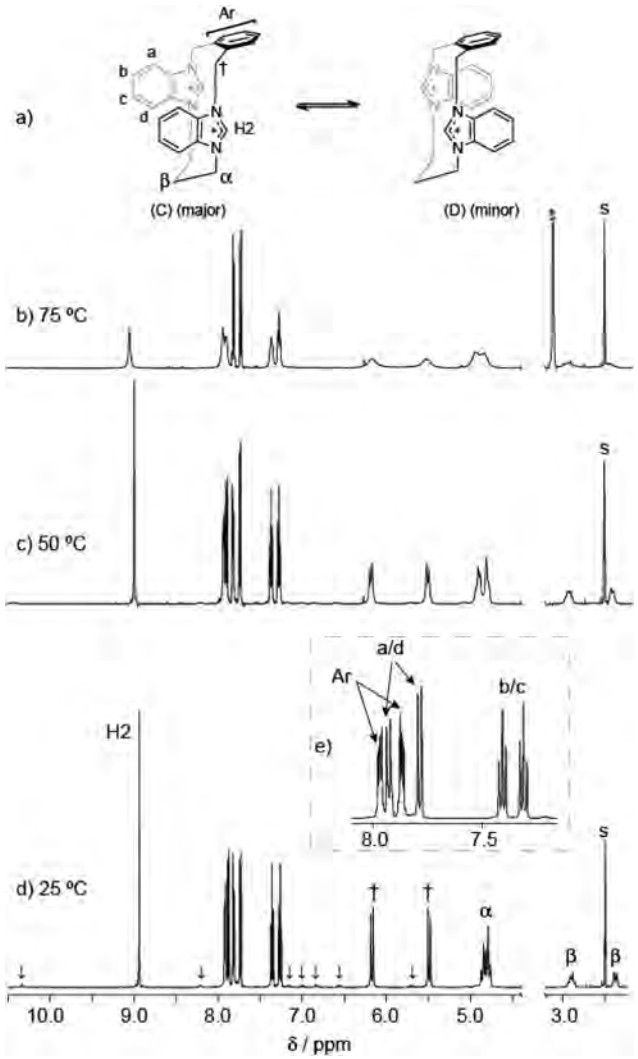

Fig. 4 Variable temperature ^{1}H NMR study of **IV**·2Br. (a) Interconversion of the (A) and (B) conformations of $\mathbf{II}^{2+}$. The conformation of the C_3 chain could not be determined by ^{1}H NMR and for illustrative convenience is based on that seen in the X-ray study. (b)–(d) ^{1}H NMR spectra (500.1 MHz, DMSO-d_6) of **IV**·2Br at 75, 50, and 25 °C respectively. (e) Expansion of the aromatic region of the spectrum in (d). In (d) and (e), labels identify signals due to the major conformation (A) and arrows highlight signals due to the minor conformation (B). The signal due to adventitious water is labelled with an asterisk, (*) and the residual solvent signal is labelled "s".

The ^{1}H NMR spectra of solutions of **III**·2Br and **V**·2Br at room temperature showed signals consistent with the cations $\mathbf{III}^{2+}$ and $\mathbf{V}^{2+}$ existing as rapidly interconverting conformations (see ESI, Fig. S4 and S5†). For example, in both cases, the benzylic protons of the xylyl group appeared as sharp singlets, not the AX doublet patterns characteristic of benzylic protons in conformationally rigid azolium cyclophanes. Evidently, the larger macrocycle size provided by the presence of the C_4 linker in $\mathbf{III}^{2+}$ and $\mathbf{V}^{2+}$ facilitates interconversion of conformations, presumably *via* processes involving rotation of the azolium groups about their N—N axes, allowing the H2 end of the azolium group to swing through the macrocyclic ring. The ^{1}H NMR spectra for $\mathbf{III}^{2+}$ and $\mathbf{V}^{2+}$ broadened at low temperatures, but even at −60 °C (for $\mathbf{III}^{2+}$) and −75 °C (for $\mathbf{V}^{2+}$) the exchange processes were not slowed sufficiently for signals due to individual conformations to be observed.

Au(I)–NHC complexes

Synthesis and NMR spectroscopy. In a similar fashion to that used for the preparation of **1**·2Br,[27] heating a 1 : 1 mixture of an azolium cyclophane salt (**III**·2Br, **IV**·2Br or **V**·2Br) and an Au(I) source ($(CH_3)_2SAuBr$) in the presence of a mild base (sodium acetate) afforded Au(I)–NHC complexes $\mathbf{2}^{2+}$, $\mathbf{3}^{2+}$, and $\mathbf{4}^{2+}$ respectively (Scheme 2) as their bromide salts. The complexes are of general form $Au_2L_2^{2+}$, where L is a cyclophane bis(NHC) ligand. In each case, two stereoisomers of each cation were generated as a consequence of the asymmetry in the ligands, a *cis* isomer where the cyclophane supporting ligands are arranged with their *o*-xylyl groups on the same side of the plane defined by the carbene C atoms, and a *trans* isomer where the *o*-xylyl groups are on the opposite sides of this plane. Numerous attempts to synthesize Au(I) complexes from the C_2-linked cyclophane **I**·2Br afforded only intractable solids.

The ^{1}H NMR spectra were as expected for complexes of form $Au_2L_2^{2+}$ that are rigid in solution.[13] For example, the benzylic protons of the xylyl groups in each complex appeared as a pair of doublets, a pattern characteristic for cyclophane bis(NHC) complexes in which each benzylic carbon carries protons in non-equivalent *endo* and *exo* environments.[11,13] Due to the symmetry properties of each complex (*cis* isomers, one two-fold proper rotation axis and two vertical reflection planes, point group C_{2v}; *trans* isomers, one two-fold proper

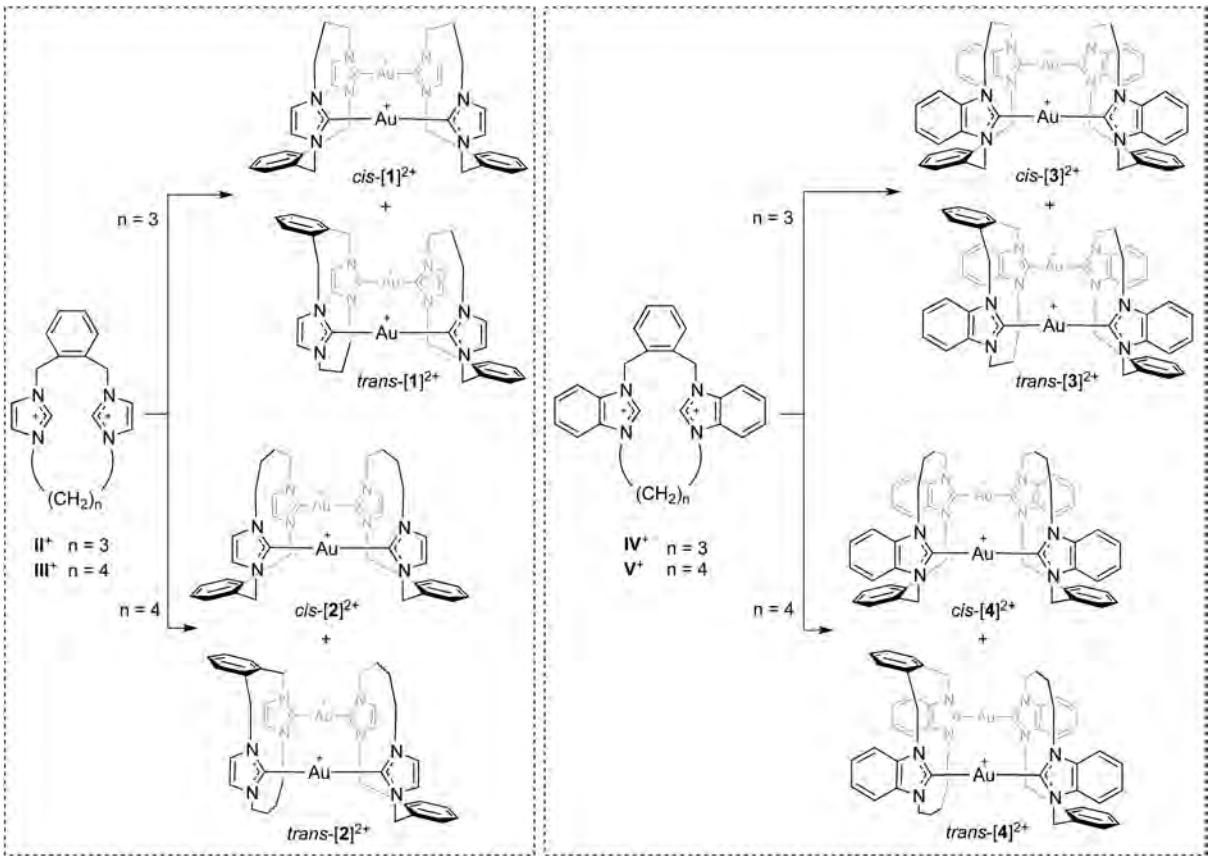

Scheme 2

rotation axis and one horizontal reflection plane, point group C_{2h}) NMR spectra of *cis* and *trans* isomers each showed the same number of signals, which had similar chemical shifts and splitting patterns, so the stereochemistry of each complex could not be readily assigned by NMR spectroscopy.

X-ray crystallography. X-Ray diffraction studies were undertaken for crystals of *cis*-**2**·BrCl·3H_2O, *trans*-**2**·$Br_{0.75}Cl_{1.25}$·4MeOH·2H_2O, *cis*-**3**·2Br·2MeOH·3H_2O, *cis*-**4**·2Br·2MeOH and *trans*-**4**·2Br·3MeOH, containing the cations *cis*-$\mathbf{2}^{2+}$, *trans*-$\mathbf{2}^{2+}$, *cis*-$\mathbf{3}^{2+}$, *cis*-$\mathbf{4}^{2+}$ and *trans*-$\mathbf{4}^{2+}$ respectively. The structures of the cations are shown in Fig. 5 and 6, while selected bond lengths and angles obtained are given in Table 2, along with those of the cations *cis*-$\mathbf{1}^{2+}$, *trans*-$\mathbf{1}^{2+}$, and $\mathbf{5}^{2+}$ reported previously.[13,27]

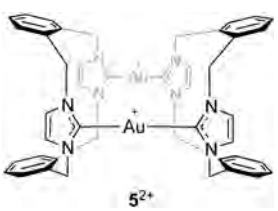

$\mathbf{5}^{2+}$

All of the new compounds contained a dinuclear cation of form $Au_2L_2^{2+}$ (L = cyclophane bis(NHC) ligand), two halide counterions, and solvent molecules. In the cation, the *o*-xylyl groups are splayed away from the Au atoms, as has been found previously in all other $Au_2L_2^{2+}$,[13] $Ag_2L_2^{2+}$,[39] and $Hg_2L_2^{2+}$ complexes[40] in which *o*-xylyl link the NHC moieties. While the Au–C2 distances are unexceptional, Au···Au distances are short in all the cations, consistent with there being aurophilic interactions between the Au centres. The Au···Au distance appears to be largely determined by the nature of the groups linking the NHC units, being shorter in the complexes with one *o*-xylyl and one C_3-linker (*cis*- and *trans*-$\mathbf{1}^{2+}$ and *cis*-$\mathbf{3}^{2+}$, average ~2.940 Å) and longer in the complexes with one *o*-xylyl and one C_4 linker (*cis*- and *trans*-$\mathbf{2}^{2+}$ and *cis*- and *trans*-$\mathbf{4}^{2+}$, average ~3.198 Å). In complex $\mathbf{5}^{2+}$, having two *o*-xylyl linkers, the Au···Au distance falls in between (3.0485 Å), presumably because the larger C–C–C bond angles and shorter arene C–C bond in the C_4 linking portion of the *o*-xylyl unit result in the *o*-xylyl unit being effectively "shorter" than the simple tetramethylene C_4 group. Interestingly, for the cations $\mathbf{2}^{2+}$ and $\mathbf{4}^{2+}$, both of which contain a C_4 linker, the Au···Au distance is significantly longer in the *cis* isomer than in the *trans* isomer. In all the cations, the planes of the NHC groups in each cyclophane slightly tilt towards each other at their carbene ends, as indicated by C2–Au–C2 angles in the range 173.0–179.4°.

For *cis*-**2**·BrCl·3H_2O, the anionic sites were modelled as being partially occupied by chloride and bromide ions (site 1),

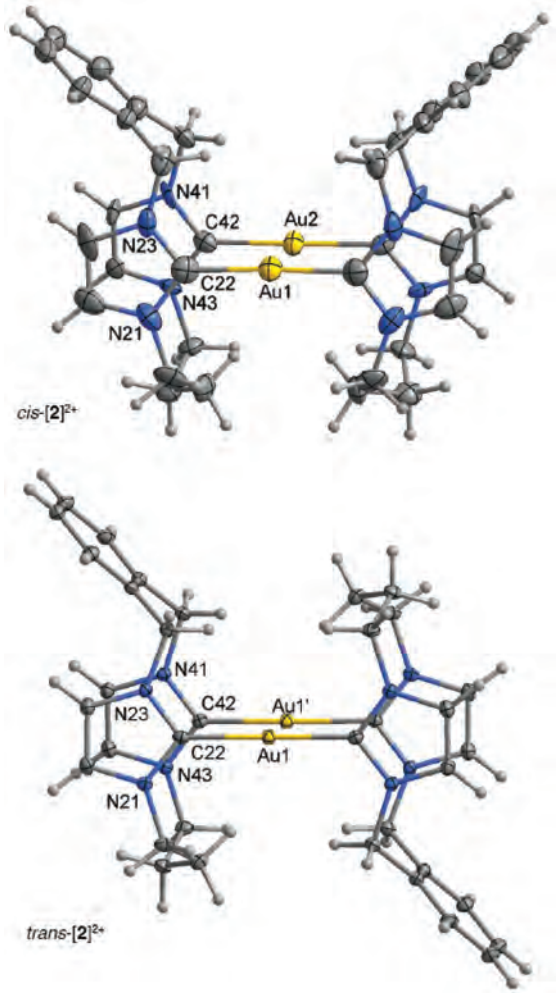

Fig. 5 Structures of cations *cis*-$[\mathbf{2}]^{2+}$ and *trans*-$[\mathbf{2}]^{2+}$, containing imidazolyl-derived C_4-linked cyclophane ligands. Unit cell contents are shown in the ESI, Fig. S6.†

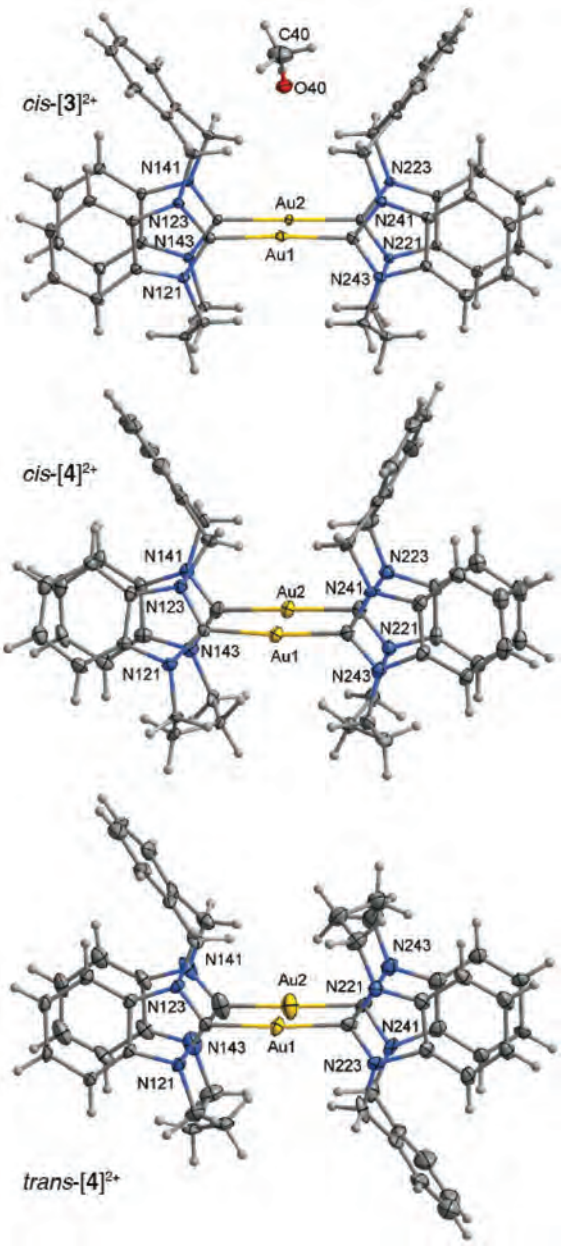

Fig. 6 Structures of cations *cis*-$[\mathbf{3}]^{2+}$, *cis*-$[\mathbf{4}]^{2+}$, and *trans*-$[\mathbf{4}]^{2+}$, containing benzimidazolyl-derived cyclophane ligands. For *cis*-$[\mathbf{3}]^{2+}$ (C_3-linked), a molecule of methanol is shown co-crystallised inside the 'cups' formed by the two *o*-xylyl groups. For both *cis*-$[\mathbf{4}]^{2+}$ and *trans*-$[\mathbf{4}]^{2+}$ (C_4-linked), only one component of the disordered atoms has been included. Unit cell contents are shown in the ESI, Fig. S7.†

bromide ions and water (site 2), or chloride ions and water (site 3), with occupancies set at 0.5 after trial refinement. The cation *cis*-$\mathbf{2}^{2+}$ is situated on a crystallographic mirror plane perpendicular to the crystallographic *a* axis, and the unit cell projection (ESI, Fig. S6a†) shows that the cations lie parallel to the *ac* plane, alternating with planes containing counter ions and water molecules. For *trans*-$\mathbf{2}\cdot Br_{0.75}Cl_{1.25}\cdot 4MeOH\cdot 2H_2O$, the anions were refined as part bromide and part chloride, with the occupancies refined to 0.624(2) and 1–0.624(2) for chloride and bromide, respectively. The cation *trans*-$\mathbf{2}^{2+}$ lies on a crystallographic inversion centre. The halide counter ions in the lattice, as well as the water and methanol molecules, form a hydrogen bonded cluster around the cell origins as shown in the cell projected along the *a* axis (ESI, Fig. S6b†).

For *cis*-$\mathbf{3}\cdot 2Br\cdot 2MeOH\cdot H_2O$, containing benzimidazolyl C_3-linked cyclophane ligands, one methanol molecule crystallised inside the 'cup' formed by the *o*-xylyl groups (Fig. 6a). The unit cell projection along the *b* axis (ESI, Fig. S7a†) shows that the cations lie in sheets, parallel to the *bc* plane, and alternate with sheets containing bromide ions, methanol, and water molecules.

The atoms of the C_4 linker in the cation *cis*-$\mathbf{4}^{2+}$ were disordered over two sites, with occupancies refined to 0.708(3) and its complement. The solvent was modelled as two methanol molecules (not shown), both disordered over two sets of sites, with occupancies constrained, after trial refinement, to be the same as the disordered C_4 moiety. The unit cell diagram for *cis*-$\mathbf{4}\cdot 2Br\cdot 3MeOH$, projected along the *a* axis (ESI,

Table 2 Selected bond lengths and angles for the dinuclear Au(I)–NHC complexes

Cation	Space group	Au–C2$_{22/42}$ (Å)	C2–Au–C2 (°)	Au(I)···Au(I) (Å)
cis-**1**$^{2+}$ [a]	*C*2/*c*	2.035(6), 2.033(6)	177.4(3)	2.9290(4)
trans-**1**$^{2+}$ [a]	*C*2/*c*	2.036(6), 2.029(6)	175.5(3)	2.9582(4)
cis-**2**$^{2+}$ [b]	$Pmc2_1$	1.963(9), 2.051(7)	177.0(5), 176.8(4)	3.2880(6)
trans-**2**$^{2+}$ [c]	$P\bar{1}$	2.0239(17), 2.0216(17)	176.07(7)	3.1402(4)
cis-**3**$^{2+}$ [d]	$P\bar{1}$	2.0276(19), 2.033(2), 2.0266(18), 2.0269(19)	174.84(8), 179.44(7)	2.93289(12)
cis-**4**$^{2+}$ [e]	$C222_1$	2.028(3), 2.034(4), 2.029(4), 2.030(4)	174.19(15), 177.66(15)	3.2318(2)
trans-**4**$^{2+}$ [f]	$P2_1/n$	2.021(16), 2.035(17), 1.97(2), 2.077(18)	176.5(8), 176.3(7)	3.1301(11)
5^{2+} [g]	$Pca2_1$	1.997(5), 2.066(6) 1.979(6), 2.061(6)	173.0(2) 176.9(2)	3.0485(3)

[a] Crystal structure for (*cis*-**1**,*trans*-**1**·4Br·2′H_2O′)$_{0.5}$ = $C_{34}H_{38}Au_2Br_2N_8O$.[27] [b] Crystal structure for *cis*-**2**·BrCl·3H_2O. [c] Crystal structure for *trans*-**2**·$Br_{0.75}Cl_{1.75}$·4MeOH·2H_2O. [d] Crystal structure for *cis*-**3**·2Br·2MeOH·3H_2O. [e] Crystal structure for *cis*-**4**·2Br·2MeOH. [f] Crystal structure for *trans*-**4**·2Br·3MeOH. [g] Crystal structure for *trans*-**5**·2Br·2MeCN.[13]

Fig. S7b†) shows a weak interaction between Br(1) and Au(2) atoms of adjacent cations, with the shortest Br(1)–Au(2) distance found to be 3.9559(2) Å. The crystal structure of *trans*-**4**·2Br·3MeOH contained bromide counter ions that are disordered over five sites, with the sum of their occupancies constrained to be 2. The three solvent molecules (methanol), in which the hydroxyl hydrogens were refined as part of riding models, were restrained for possible hydrogen bonding to Br(3) and Br(4). Furthermore, the central two C atoms of the C_4 linker of *trans*-**4**$^{2+}$ were disordered over two sets of sites, with occupancies set to 0.5 after a trial refinement. The unit cell contents for *trans*-**4**·2Br·3MeOH is shown in Fig. S7c (ESI†).

Luminescence characteristics. The solution luminescence behaviour of *cis*-**1**·2Br and *trans*-**1**·2Br has been reported previously.[27] We found that aqueous solutions of *cis*-**3**·2Br and *trans*-**3**·2Br also exhibited intense luminescence, most likely due to the close proximity of the Au(I) centres ions at the core of the complex (Au···Au ~ 2.9 Å in the crystal structure). The luminescence excitation and emission spectra for aqueous solutions of the *cis*-**3**·2Br are shown in Fig. 7; those for *trans*-**3**·2Br were essentially identical. The electronic absorption spectrum shows two main bands, centred at 288 and 345 nm. The luminescence emission spectrum (λ_{ex} = 288 nm) shows a strong band at 431 nm and a weaker band at 555 nm. The excitation spectrum (λ_{em} = 431 nm) is very similar to the electronic absorption spectrum, with maxima at 288 and 345 nm. The emission quantum yields (Φ) are 0.63 (λ_{ex} = 288 nm) and 0.84 (λ_{ex} = 345 nm) when relative to quinine sulfate.[41,42] Complexes **2**.2(Br/Cl) and **4**·2Br, bearing the cyclophane supporting ligands with C_4-linked alkyl chains, were found to have significantly longer intramolecular Au···Au distances in the solid state (~3.3 Å). While complexes **2**.2(Br/Cl) and **4**·2Br displayed luminescence in aqueous solution, luminescence measurements were difficult due to their low solubility. The higher luminescence of solutions containing the C_3-linked cyclophane complexes *cis*-**1**$^{2+}$ or *cis*-**3**$^{2+}$ compared to that for solutions containing the C_4-linked cyclophane complexes *cis*-**2**$^{2+}$ or *cis*-**4**$^{2+}$ can be seen qualitatively by illumination of solutions with a TLC lamp (Fig. S8†).

Biological studies of Au^{I}–NHC complexes. All attempts to measure cytotoxicity of bromide salts of *cis* and *trans* isomers of **2**$^{2+}$ and **4**$^{2+}$ in HeLa cells resulted in large crystals of the

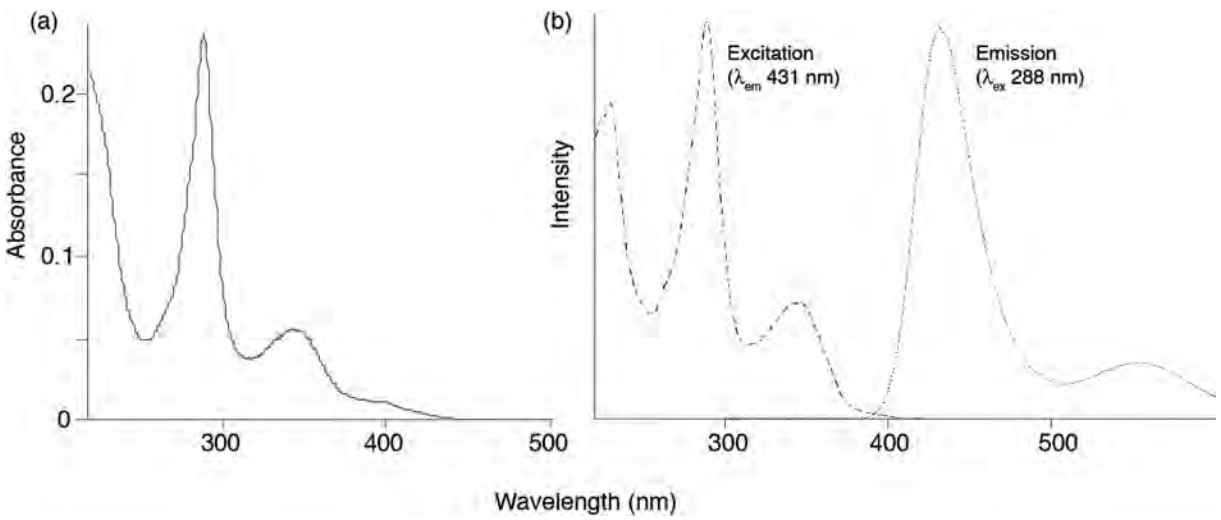

Fig. 7 (a) Electronic absorption and (b) luminescence excitation (dashed line, λ_{em} = 431 nm) and emission (dotted line, λ_{ex} = 288 nm) spectra for *cis*-**3**·2Br (5 μM in water).

Au–NHC complexes appearing in the culture wells. For this reason, representative cell proliferation studies were carried out on HeLa cells using the *cis* and *trans* isomers of the Au complexes **1**·2Br and **3**·2Br only. The CellTiter 96® Aqueous One Solution Reagent assay was used, based on the reduction of a tetrazolium ion ([3-(4,5-dimethylthiazol-2-yl)-5-(3-carboxymethoxyphenyl)-2-(4-sulfophenyl)-2*H*-tetrazolium, MTS) to a coloured formazan product only in healthy and metabolically active cells, and the results are shown in Fig. S9.† The data showed that *cis*-**1**·2Br and *trans*-**1**·2Br caused a decrease in the number of viable HeLa cells in culture to *ca.* 60% at concentrations of 100 μM and 75 μM, respectively, over a period of 24 h. Similarly, *cis*-**3**·2Br and *trans*-**3**·2Br caused a decrease in the percentage of viable cells to *ca.* 60% at 82 μM and 75 μM, respectively. These data show that these Au–NHC complexes have low cytotoxicity (IC_{50} values >100 μM) in HeLa cells.

The lipophilicity of the *cis* isomers of each of Au–NHC complexes (Table 3) was assessed using the octanol–water partition coefficient, log *P*.[43] All of the complexes have hydrophilic character with log *P* < 0. Furthermore, the results show that the incorporation of the extra CH_2 group into the alkyl linker of the supporting cyclophane ligands does not result in a significant change in log *P* for the resultant Au–NHC complex. Incorporation of the extra aromatic rings in the benzimidazole-derived complexes, however, resulted in a significant increase in hydrophobic character, as indicated by an increase in log *P* of ~1 unit.

Complexes *cis*-**3**·2Br and *trans*-**3**·2Br showed aqueous solution luminescence characteristics suitable for identifying their sub-cellular localization inside live cells. MDA-MB-231 (MDA) breast cancer cells were treated with *cis*-**3**·2Br (final concentration 26.2 μM) and the cells were visualized using a luminescence microscope for 6 h (UV illumination, one image recorded every 30 s), and the time lapse movie of the cellular uptake and localization is provided in ESI (Movie S1†). No photo-bleaching of the luminescence originating from *cis*-**3**·2Br was apparent over the duration of the experiment. Two images recorded 1 h and 3 h after initial exposure of cells to *cis*-**3**·2Br are shown in Fig. 8. There is increasing luminescence intensity from cells after addition of *cis*-**3**·2Br, an indication of cellular uptake of the luminescent Au–NHC complex. After 3 h, the luminescence signal appeared punctate, and localised to small subcellular compartments, likely endosomes or lysosomes. In some of the cells there was a central region devoid of luminescence, suggesting that the compound does not accumulate in the nuclei of cells. Movie S1† shows remarkably detailed capture of the live cellular processes as the cells take up *cis*-**3**·2Br. After 1 h, diffuse luminescence was seen originating from nearly all of the cells in the field of view, with very intense luminescence originating from some cells. After 3 h, whilst the diffuse luminescence intensity remained throughout the cells, there was the accumulation of intense luminescence signal originating from small and highly mobile organelles. Whilst the organelles have not been identified in these experiments, our previous studies using *cis*-**1**·2Br (100 μM) and $RAW_{264.7}$ cells (15 h incubation) showed localization to lysosomes rather than mitochondria, suggesting that they are sequestered there for degradation. Notably the greater lipophilicity of *cis*-**3**·2Br allowed cellular imaging studies to be carried out with a 4-fold lower concentration and with luminescence visible in a much shorter timeframe (less than 1 h).

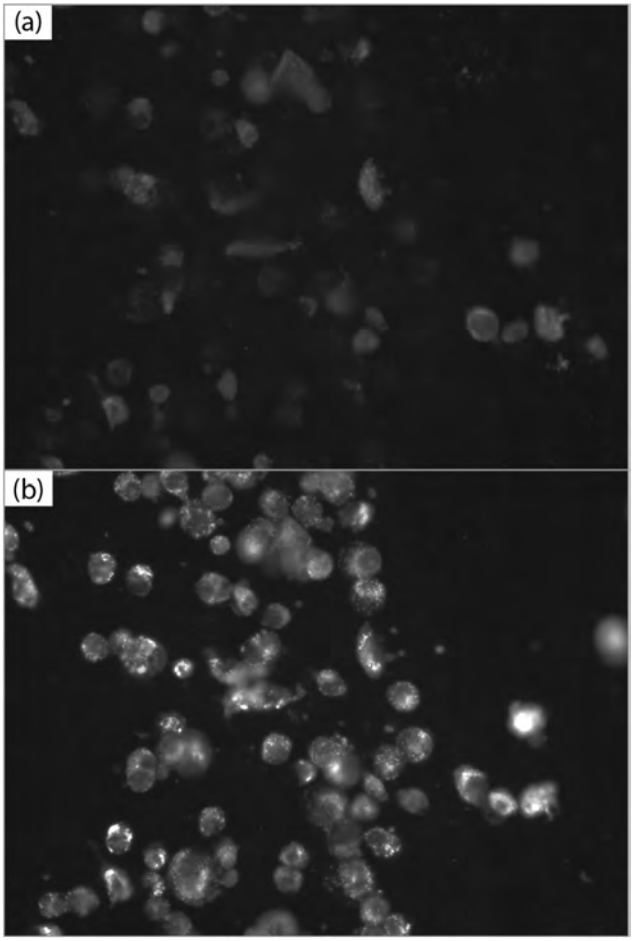

Fig. 8 Luminescence microscopy images of MDA-MB-231 cells (a) 1 h (b) 3 h after treatment with *cis*-**3**·2Br (26.2 μM). No background fluorescence was observed before addition of *cis*-**3**·2Br.

Table 3 log *P* values determined for the *cis* isomers of the dinuclear Au(I) cyclophane complexes

Complex	log *P*
cis-**1**·2Br	−2.36 ± 0.23
cis-**2**·2Br	−2.35 ± 0.21
cis-**3**·2Br	−1.15 ± 0.04
cis-**4**·2Br	−1.10 ± 0.06

Conclusions

In solution of their dibromide salts, the cyclophane cations $\mathbf{I}^{2+}$–$\mathbf{V}^{2+}$ were fluxional on the NMR timescale. For the C_3-linked

cyclophanes $\mathbf{II}^{2+}$ and $\mathbf{IV}^{2+}$, fluxionality was due to interconversion of conformations in which the azolium groups were mutually *syn*. For the C_4-linked cyclophanes $\mathbf{III}^{2+}$ and $\mathbf{V}^{2+}$, interconversion between conformations in solution occurred too rapidly for the individual conformations to be identified, but in the solid state both cyclophanes adopted conformations in which the azolium groups were mutually *syn*. For the C_2-linked cyclophane $\mathbf{I}^{2+}$, in solution and in the solid state, only conformations in which the imidazolium groups were mutually *anti* were detected.

The C_2-linked cyclophane **I**·2Br could not be converted into a dinuclear complex of form $Au_2L_2^{2+}$, perhaps a consequence of $\mathbf{I}^{2+}$ (or its NHC derivatives) being unable to adopt a conformation in which the heterocyclic units are mutually *syn*. The C_3- and C_4-linked cyclophanes were readily converted into the dinuclear Au–NHC complexes $\mathbf{1}^{2+}$–$\mathbf{4}^{2+}$, each of which existed as *cis* and *trans* isomers due to the asymmetry in the cyclophane structure. We have shown in this work that by appropriate ligand design, we have been able to construct complexes having short Au···Au contacts, between ~2.9 and ~3.3 Å, indicative of an aurophilic interaction.[29] In parallel, modification of the supporting cyclophane structure to incorporate less polar functional groups significantly influenced the lipophilicity of the complexes, to in turn influence membrane solubility of the complexes, and their cellular uptake and distribution patterns. The luminescent properties of *cis*-**3**·2Br were exploited to map the distribution of the complex inside live tumour cells, without the need for an additional fluorescent tag, giving valuable insight into the sub-cellular distribution for this class of compounds. Notably the observation of intense fluorescence inside the cells over a period of 6 h indicates the integrity of the dinuclear complex (*i.e.* Au(I)···Au(I) distance) remains intact and it is not degraded by *in cellulo* reactions with biological thiols, consistent with the lack of reactivity of *cis*-**1**·2Br with glutathione.[27] In turn, the low thiol reactivity is consistent with the low cytotoxicity of these dinuclear Au–NHC complexes, in comparison with mononuclear Au(I)–NHC complexes, where antitumour activity has been attributed to facile ligand exchange reactions with protein thiols and selenols, such as TrxR.[24]

Optical probes for use in biological systems should enter the cell quickly, cause minimal perturbation of the cell, maintain their integrity and remain emissive once inside the cell, and resist photofading/photobleaching.[44] Since the luminescence signal originating from *cis*-**3**·2Br was resistant to photobleaching for more than 6 h, and as *cis*-**3**·2Br was not significantly cytotoxic, complexes of this type may have potential applications as emissive molecular probes. Metal coordination complexes offer many advantages as cell penetrating optical probes, including design versatility not available in purely organic molecules. Fine-tuning the design of these Au–NHC complexes (for example by incorporation of peptide conjugates)[45,46] provides ample scope to improve targeting of probes to specific cells or subcellular organelles.

Experimental

General information

All chemical reagents and solvents were obtained from commercial sources (Univar, Aldrich or Fluka) unless otherwise specified. Au powder was obtained from Precious Metals Online. Nuclear magnetic resonance spectra were recorded using Bruker ARX-300 (300.14 MHz for ^{1}H), Bruker AV-500 (500.13 MHz for ^{1}H), or Bruker AV-600 (600.13 MHz for ^{1}H) spectrometers at ambient temperature unless stated otherwise. ^{1}H NMR chemical shifts were referenced to solvent references.[47] Microanalyses were performed by the Microanalytical Laboratory at the Research School of Chemistry, Australian National University, Canberra. Solvents for synthetic work were purified by distillation from the appropriate drying agent under nitrogen, and stored over sieves when necessary.[48] α,α′-Dibromo-*o*-xylene,[49] 1,2-bis(*N*-imidazolyl)ethane,[50] 1,3-bis(*N*-imidazolyl)propane,[51] 1,4-bis(*N*-imidazolyl)butane,[52] 1,3-bis(*N*-benzimidazolyl)propane,[53] 1,4-bis(*N*-benzimidazolyl)butane,[53] **II**·2Br,[27] and (Me_2S)AuCl,[54] were prepared according to literature procedures. (Me_2S)AuBr was prepared by the addition of Me_2S (2 equivalents) to $KAuBr_4$ in a modification of the procedure used for (Me_2S)AuCl.

Synthesis of azolium cyclophane salts. I·2Br: Acetonitrile solutions (150 mL) of 1,2-bis(*N*-imidazolyl)ethane (3 g, 18.5 mmol) and α,α′-dibromo-*o*-xylene (4.88 g, 18.5 mmol) were added simultaneously and dropwise to refluxing acetonitrile (450 mL) over a period of 6 h, and the mixture was left to reflux overnight. The resulting cloudy, white mixture was cooled to room temperature and filtered, and the solvent was removed under reduced pressure, yielding a white solid. Recrystallisation from ethanol yielded colourless crystals of **I**·2Br (1.35 g, 27%), which were collected at the pump and washed with diethyl ether. ^{1}H NMR (300.13 MHz, DMSO-d_6): δ = 7.98 (t, $^4J_{HH}$ = 1.68 Hz, 2H, imidazolyl H2), 7.95 (t, $^3J_{HH}$ = 1.7 Hz, 2H, imidazolyl H4/5), 7.82–7.9 (m, 2H, xylyl ArH), 7.60–7.67 (m, 2H, xylyl ArH), 7.43 (t, $^3J_{HH}$ = 1.7 Hz, 2H, imidazolyl H4/5) 5.72 (d, $^2J_{HH}$ = 14.4 Hz, 2H, xylyl CH*H*), 5.62 (d, $^2J_{HH}$ = 14.4 Hz, 2H, xylyl C*H*H), 4.77 (apparent d, splitting = 10.4 Hz, 2H, CH*H*CH*H*), 4.22 (apparent d, splitting = 10.4 Hz, 2H, C*H*HC*H*H). Elem. Anal.: Calcd for $C_{16}H_{18}N_4Br_2{\cdot}0.5H_2O{\cdot}0.5CH_3CH_2OH$: C 44.56, H 4.83, N 12.22. Found: C 44.66, H 4.65, N 12.54.

III·2Br: Acetonitrile solutions (50 mL) of 1,4-bis(*N*-imidazolyl)butane (0.95 g, 5.0 mmol) and α,α′-dibromo-*o*-xylene (1.3 g, 5.0 mmol) were added simultaneously and dropwise to refluxing acetonitrile (250 mL) over a period of 6 h, and the mixture was allowed to reflux for a further 72 h, during which time a white insoluble solid deposited on the reaction flask. The mixture was filtered whilst hot to yield a clear yellow filtrate. The solvent was removed from the filtrate under reduced pressure to yield a white solid. Recrystallised from boiling ethanol afforded large colourless crystals of **III**·2Br (1.27 g, 56%), which were collected at the pump and washed with cold diethyl ether. ^{1}H NMR (500.13 MHz, CD_3OD): δ = 7.80–7.84 (m, 2H, xylyl ArH), 7.70–7.74 (m, 2H, xylyl ArH), 7.54 (d, $^3J_{HH}$ = 2.0 Hz, 2H, imidazo-

lyl H4/5), 7.48 (d, $^3J_{HH}$ = 2.0 Hz, 2H, imidazolyl H4/5), 5.69 (s, 4H, xylyl CH_2), 4.15 (apparent t, splitting = 5 Hz, 4H, NCH_2CH$_2$CH$_2$CH_2N), 1.98 (apparent quintet, splitting = 5 Hz, 4H, NCH$_2$CH_2CH_2CH$_2$N). The imidazolyl H2 proton was not seen due to H/D exchange, but in DMSO-d_6 solution was seen as a singlet at δ 8.60. Elem. Anal.: Calcd for $C_{18}H_{22}N_4Br_2{\cdot}1.5H_2O$: C 44.93, H 5.23, N 11.64. Found: C 45.29, H 5.33, N 11.57.

IV·2Br: Acetonitrile solutions (50 mL) of 1,3-bis(*N*-benzimidazolyl)propane (1.0 g, 35.7 mmol) and α,α′-dibromo-*o*-xylene (0.94 g, 35.0 mmol) were added simultaneously and dropwise to refluxing acetonitrile (200 mL) over a period of 6 h, and the solution was allowed to reflux for a further 72 h. The mixture was filtered whilst hot and the clear yellow filtrate was stripped of solvent under reduced pressure to yield a white solid. Recrystallisation from boiling ethanol gave colourless crystals of **IV**·2Br (1.68 g, 89%), which were collected at the pump and washed with cold diethyl ether. ^{1}H NMR (500.13 MHz, DMSO-d_6): δ = 8.94 (s, 2H, benzimidazolyl H2), 7.90–7.94 (m, 2H, xylyl ArH), 7.79–7.85 (m, 2H, xylyl ArH), 7.88 (dd, $^3J_{HH}$ = 8.0 Hz, $^4J_{HH}$ = 0.8 Hz, 2H, benzimidazolyl H4/7), 7.73 (dd, $^3J_{HH}$ = 8.0 Hz, $^4J_{HH}$ = 0.8 Hz, 2H, benzimidazolyl H4/7), 7.36 (dt, $^3J_{HH}$ = 8.0 Hz, $^4J_{HH}$ = 0.8 Hz, 2H, benzimidazolyl H5/6), 7.26 (dt, $^3J_{HH}$ = 8.0 Hz, $^4J_{HH}$ = 0.8 Hz, 2H, benzimidazolyl H5/6), 6.18 (d, $^2J_{HH}$ = 14.6 Hz, 2H, xylyl CH*H*), 5.49 (d, $^2J_{HH}$ = 14.6 Hz, 2H xylyl C*H*H), 4.75 (m, 4H, NCH_2CH$_2$CH_2N), 2.86 (m, 1H, NCH$_2$C*H*HCH$_2$N), 2.34 (apparent d, splitting = 16.0 Hz, 1H, NCH$_2$CH*H*CH$_2$N). Elem. Anal.: Calcd for $C_{25}H_{24}N_4Br_2{\cdot}2.5H_2O$: C 51.30, H 4.99, N 9.76. Found: C 51.67, H 4.95, N 9.76.

V·2Br: Acetonitrile solutions (75 mL) of 1,4-bis(*N*-benzimidazolyl)butane (1.0 g, 3.4 mmol) and α,α′-dibromo-*o*-xylene (0.9 g, 3.4 mmol) were added simultaneously and dropwise to refluxing acetonitrile (200 mL) over a period of 6 h, and the mixture was allowed to reflux for a further 48 h, during which time a white precipitate formed. The mixture was filtered whilst hot and the collected solid was suspended in boiling ethanol (50 mL) for 15 min. The suspension was filtered whilst hot, and from the resulting yellow solution, large colourless crystals of **V**·2Br (0.53 g, 22%) were deposited upon cooling. The crystals were collected at the pump and washed with diethyl ether. ^{1}H NMR (500.13 MHz, DMSO-d_6): δ = 8.96 (s, 2H, benzimidazolyl H2), 7.88–7.92 (m, 2H, xylyl ArH), 7.77–7.82 (m, 2H, xylyl ArH), 7.96 (d, $^3J_{HH}$ = 8.5 Hz, 2H, benzimidazolyl H4/7), 7.68 (d, $^3J_{HH}$ = 8.5 Hz, 2H, benzimidazolyl H4/7), 7.41 (dt, $^3J_{HH}$ = 8.5 Hz, $^4J_{HH}$ = 1.0 Hz, 2H, benzimidazolyl H5/6), 7.30 (dt, $^3J_{HH}$ = 8.5 Hz, $^4J_{HH}$ = 1.0 Hz, 2H, benzimidazolyl H5/6), 5.86 (br, 4H, xylyl CH_2), 4.31 (br, 4H, NCH_2CH$_2$CH$_2$CH_2N), 2.05 (br, 4H, NCH$_2$CH_2CH_2CH$_2$N). Elem. Anal.: Calcd for $C_{26}H_{26}N_4Br_2{\cdot}0.5H_2O$: C 55.44, H 4.83, N 9.94. Found: C 55.53, H 4.89, N 9.83.

Synthesis of Au–NHC complexes. 2·2Br: **III**·2Br (199 mg, 0.44 mmol) and (Me_2S)AuCl (129 mg, 0.44 mmol) were dissolved in hot DMF (40 mL, 95 °C). Sodium acetate (0.11 g, 1.3 mmol) was added and heating was continued for a further 24 h, during which time a white precipitate formed. The mixture was allowed to cool, and the white precipitate was collected at the pump and washed with diethyl ether. The filtrate was poured into diethyl ether (200 mL) to produce a second white precipitate, which was collected at the pump and washed with acetone then diethyl ether. The first precipitate was recrystallised from boiling methanol and isopropanol (5 : 1) to give *trans*-**2**·2Br as colourless needles. These crystals were collected at the pump and washed with acetone (11 mg, 4.4%). The second white precipitate that formed on addition of diethyl ether to the filtrate was recrystallised from boiling methanol/isopropanol (5 : 1) to give white microcrystals of *cis*-**2**·2Br, which were collected and washed with acetone (28 mg, 11%). *cis*-**2**·2Br: ^{1}H NMR (500.13 MHz, CD_3OD): δ = 7.75–7.79 (m, 4H, xylyl ArH), 7.65–7.69 (m, 4H, xylyl ArH), 6.99 (d, $^3J_{HH}$ = 2.0 Hz, 4H, imidazolyl H4/5), 6.65 (d, $^3J_{HH}$ = 2.0 Hz, 4H, imidazolyl H4/5), 6.43 (d, $^2J_{HH}$ = 14.0 Hz, 4H, xylyl C*H*H), 5.26 (d, $^2J_{HH}$ = 14.0 Hz, 4H, xylyl CH*H*), 4.42 (dd, $^2J_{HH}$ = 14.5 Hz, $^3J_{HH}$ = 7.0 Hz, 4H, NC*H*HCH$_2$CH$_2$C*H*HN), 4.05 (dd, ^2J = 14.5 Hz, ^3J = 7.0 Hz, 4H, NCH*H*CH$_2$CH$_2$CH*H*N), 2.94 (m, 4H, NCH$_2$C*H*HCH*H*CH$_2$N), 2.16 (m, 4H, NCH$_2$CH*H*CH*H*CH$_2$N). Elem. Anal.: Calcd for $C_{36}H_{40}Au_2N_8Br_2(H_2O)_3$: C 36.26, H 3.89, N 9.39. Found: C 36.38, H 3.94, N 9.30.

To ensure incorporation of bromide as the counter ion, a sample of *trans*-**2**·2Br was prepared in a procedure analogous to that above, from sodium acetate (145 mg, 177 mmol), **III**·2Br (267 mg, 0.59 mmol) and (Me_2S)AuBr (200 mg, 0.59 mmol) in DMF at 95 °C. The mixture was stirred at 95 °C for a further 3.5 h, during which time a white precipitate appeared. Diethyl ether (200 mL) was added to the reaction mixture after brief cooling, and the precipitate was collected and washed with diethyl ether. The precipitate was recrystallised from a boiling mixture of methanol (50 mL) and isopropanol (1 mL) to yield *trans*-**2**·2Br as a white powder (33 mg, 9.9%) which was collected and washed with diethyl ether. *trans*-**2**·2Br: ^{1}H NMR (500.13 MHz, CD_3OD): δ = 7.79–7.84 (m, 4H, xylyl ArH), 7.70–7.76 (m, 4H, xylyl ArH), 7.01 (d, $^3J_{HH}$ = 2.0 Hz, 4H, imidazolyl H4/5), 6.47 (d, $^3J_{HH}$ = 2.0 Hz, 4H, imidazolyl H4/5), 6.20 (d, $^2J_{HH}$ = 14.0 Hz, 4H, xylyl CH*H*), 5.31 (d, $^2J_{HH}$ = 14.0 Hz, 4H, xylyl CH*H*), 4.49 (dd, $^2J_{HH}$ = 14.0 Hz, $^3J_{HH}$ = 7.0 Hz, 4H, NC*H*HCH$_2$CH$_2$C*H*HN), 4.04 (dd, $^2J_{HH}$ = 14.0 Hz, $^3J_{HH}$ = 7.0 Hz, 4H, NCH*H*CH$_2$CH$_2$CH*H*N), 3.01 (m, 4H, NCH$_2$C*H*HCH*H*CH$_2$N), 2.20 (m, 4H, NCH$_2$CH*H*CH*H*CH$_2$N). Elem. Anal.: Calcd for $C_{36}H_{40}Au_2N_8Br_2$: C 37.98, H 3.54, N 9.84. Found: C 37.78, H 3.76, N 9.64.

3·2Br: **IV**·2Br (226 mg, 0.42 mmol) and (Me_2S)AuBr (140 mg, 0.42 mmol) were dissolved in hot DMF (40 mL, 110 °C). Sodium acetate (120 mg, 1.48 mmol) was added and heating was continued at 110 °C for a further 2 h during, which time a pale yellow precipitate formed. The precipitate was collected whilst still hot, and the filtrate preserved. The precipitate was washed once with water and then with diethyl ether, and recrystallised from boiling methanol to yield a crop of large pale yellow crystals of *cis*-**3**·2Br (16 mg, 6%), which were collected by filtration through a pore 1 glass frit. Further standing of the mother liquor yielded small yellow needles of *cis*-**3**·2Br (29 mg, 10%, total yield 16%). The crude reaction filtrate was allowed to cool and diethyl ether (150 mL) was added. The resulting fine, vivid yellow precipitate was collected

at the pump and dissolved in boiling methanol (25 mL) and DMSO (3 mL) and filtered whilst hot, and the volume of the filtrate was reduced to ~12 mL. Upon cooling, *trans*-**3**·2Br was deposited as a fine yellow powder (23 mg, 8.2%), which was collected and washed with diethyl ether.

cis-**3**·2Br: ^{1}H NMR (500.13 MHz, DMSO-d$_6$): δ = 8.11–8.25 (m, 4H, xylyl ArH), 6.69–7.82 (m, 4H, xylyl ArH), 7.54 (d, $^3J_{HH}$ = 8.3 Hz, 4H, benzimidazolyl H4/7), 6.72 (d, $^3J_{HH}$ = 8.3 Hz, 4H, benzimidazolyl H4/7), 7.00 (dd, $^3J_{HH}$ = 7.8 Hz, $^3J_{HH}$ = 8.3 Hz, 4H, benzimidazolyl H5/6), 6.71 (dd, $^3J_{HH}$ = 7.8 Hz, $^3J_{HH}$ = 8.3 Hz, 4H, benzimidazolyl H5/6), 6.79 (d, $^2J_{HH}$ = 14.5 Hz, 4H, xylyl CH*H*), 5.72 (d, $^2J_{HH}$ = 14.5 Hz, 4H xylyl C*H*H), 5.50 (m, 4H, NC*H*HCH$_2$C*H*HN), 5.00 (m, 4H, NCH*H*CH$_2$CH*H*N), 2.71 (m, 2H, NCH$_2$CH*H*CH$_2$N), ~2.49 (NCH$_2$C*H*HCH$_2$N; obscured by solvent). Elem. Anal.: Calcd for $Au_2C_{50}H_{44}N_8Br_2{\cdot}CH_3OH$: C 45.62, H 3.60, N 8.35. Found: C 45.58, H 3.22, N 8.40.

trans-**3**·2Br: ^{1}H NMR (500.13 MHz, DMSO-d$_6$): δ = 8.20–8.30 (m, 4H, xylyl ArH), 7.80–7.90 (m, 4H, xylyl ArH), 7.51 (d, $^3J_{HH}$ = 8.5 Hz, 4H, benzimidazolyl H4/7), 6.95 (t, $^3J_{HH}$ = 7.5 Hz, $^3J_{HH}$ = 8.5 Hz, 4H, benzimidazolyl H5/6), 6.78 (t, $^3J_{HH}$ = 7.5 Hz, $^3J_{HH}$ = 8.5 Hz, 4H, benzimidazolyl H5/6), 6.74 (d, 4H, H4/H7, $^3J_{HH}$ = 8.5 Hz, benzimidazolyl H4/7), 6.73 (d, $^2J_{HH}$ = 14.5 Hz, 4H, xylyl C*H*H), 5.82 (d, $^2J_{HH}$ = 14.5 Hz, 4H, xylyl CH*H*), 5.51 (m, 4H, NC*H*HCH$_2$C*H*HN), 4.91 (m, 4H, NCH*H*CH$_2$CH*H*N), ~2.49 (NCH$_2$C*H*$_2$CH$_2$N; obscured by solvent). Elem. Anal.: Calcd for $Au_2C_{50}H_{44}N_8Br_2{\cdot}6.5H_2O$: C 42.06, H 4.02, N 7.85. Found: C 42.11, H 3.88, N 7.89.

4·2Br: **V**·2Br (248 mg, 0.45 mmol) and (Me)$_2$SAuBr (159 mg, 0.47 mmol) were dissolved in hot DMF (40 mL, 95 °C). Sodium acetate (148 mg, 1.8 mmol) was added and heating was continued for 24 h, during which time a pale yellow precipitate formed. The mixture was allowed to cool briefly and the precipitate was collected and the filtrate was kept. The precipitate was dissolved in boiling ethanol/methanol (2 : 1), and after hot filtration was concentrated and allowed to cool, upon which a fine white powder formed. This powder was recrystallised from boiling methanol to give *trans*-**4**·2Br as a white powder (16 mg, 4.6%) which was collected at the pump and washed with diethyl ether. Diethyl ether (200 mL) was added to the filtrate (kept from above) and the resulting white powder was recrystallised from boiling methanol to yield *cis*-**4**·2Br as colourless needles (31 mg, 8.8%) in two crops, which were collected at the pump and washed with diethyl ether.

cis-**4**·2Br: ^{1}H NMR (500.13 MHz, DMSO-d$_6$): δ = 8.14–8.21 (m, 4H, xylyl ArH), 7.77–7.84 (m, 4H, xylyl ArH), 7.43 (d, $^3J_{HH}$ = 8.0 Hz, 4H, benzimidazolyl H4/7), 6.94 (t, $^3J_{HH}$ = 8.0 Hz, 4H, benzimidazolyl H5/6), 6.74 (t, $^3J_{HH}$ = 8.0 Hz, 4H, benzimidazolyl H5/6), 6.58 (d, $^3J_{HH}$ = 8.5 Hz, 4H, benzimidazolyl H4/7), 6.83 (d, $^2J_{HH}$ = 14.0 Hz, 4H, xylyl C*H*H), 5.78 (d, $^2J_{HH}$ = 14.0 Hz, 4H, xylyl CH*H*), 4.50–4.68 (m, 8H, NC*H*$_2$CH$_2$CH$_2$C*H*$_2$N), 3.09 (br, 4H, NCH$_2$CH*H*CH*H*CH$_2$N), 2.36 (br, 4H, NCH$_2$C*H*HC*H*HCH$_2$N). Elem. Anal.: Calcd for $Au_2C_{52}H_{48}N_8Br_2{\cdot}7H_2O$: C 42.64, H 4.26, N 7.65. Found: C 42.4, H 3.85, N 7.29.

trans-**4**·2Br: ^{1}H NMR (500.13 MHz, DMSO-d$_6$): δ = 8.20–8.25 (m, 4H, xylyl ArH), 7.85–7.92 (m, 4H, xylyl ArH), 7.41 (d, $^3J_{HH}$ = 8.5 Hz, 4H, benzimidazolyl H4/7), 6.94 (t, $^3J_{HH}$ = 8.5 Hz, $^3J_{HH}$ = 8.0 Hz, 4H, benzimidazolyl H5/67), 6.75 (t, $^3J_{HH}$ = 8.5 Hz, $^3J_{HH}$ = 8.0 Hz, 4H, benzimidazolyl H5/6), 6.53 (d, $^3J_{HH}$ = 8.5 Hz, 4H, benzimidazolyl H4/7), 6.64 (d, $^2J_{HH}$ = 14.5 Hz, 4H, xylyl CH*H*), 5.89 (d, $^2J_{HH}$ = 14.5 Hz, 4H, xylyl C*H*H), 4.48–4.69 (m, 8H, NC*H*$_2$CH$_2$CH$_2$C*H*$_2$N), 3.10 (br, 4H, NCH$_2$CH*H*CH*H*CH$_2$N), 2.30 (br, 4H, NCH$_2$C*H*HC*H*HCH$_2$N). Elem. Anal.: Calcd for $Au_2C_{52}H_{48}N_8Br_2{\cdot}(CH_3OH)_2(H_2O)_2$: C 45.08, H 4.20, N 7.78. Found: C 45.38, H 4.03, N 7.62.

Crystallographic studies

Crystals of *cis*-**2**·BrCl·3H$_2$O and *trans*-**2**·Br$_{0.75}$Cl$_{1.25}$·4MeOH·2H$_2$O suitable for X-ray diffraction were obtained from samples of the Au–NHC complexes prepared from **IV**·2Br and (CH$_3$)$_2$SAuCl, followed by recrystallisation from hot methanolic solutions by addition of isopropanol. Crystals of *cis*-**3**·2Br·2MeOH·3H$_2$O suitable for diffraction were obtained by diffusion of diethyl ether vapour into a concentrated methanol solution of *cis*-**3**·2Br. All attempts to obtain crystals of *trans*-**3**·2Br resulted in crystals that were too small for diffraction, or which lost solvent too rapidly. Crystals of *cis*-**4**·2Br·2MeOH and *trans*-**4**·2Br·3MeOH suitable for X-ray diffraction studies were obtained by the slow cooling of a concentrated methanol solution of *cis*-**4**·2Br and diffusion of diethyl ether vapour into a concentrated methanol/DMSO solution *trans*-**4**·2Br, respectively.

X-Ray diffraction data were collected on an Oxford diffraction Xcalibur diffractometer (Oxford Diffraction Gemini for *cis*-**3**·2Br·2MeOH·3H$_2$O, Bruker Smart diffractometer for **II**·2Br·C$_3$H$_6$O·H$_2$O) fitted with Mo Kα radiation. The data for **I**·2Br·2H$_2$O were collected on a synchrotron. All of the structures presented have probability ellipsoids drawn at the 50% level (30% level for **IV**·2Br·CH$_3$CH$_2$OH and *trans*-**4**·2Br·3MeOH). Crystallographic data for the structures were collected at 100(2) K (150(2) K for **II**·2Br·C$_3$H$_6$O·H$_2$O and **IV**·2Br·CH$_3$CH$_2$OH, 103 K for **I**·2Br·2H$_2$O). Following multi-scan absorption corrections (analytical for *cis*-**3**·2Br·2MeOH·3H$_2$O) and solution by direct methods, the structures were refined against F^2 with full-matrix least-squares using the programs SHELXL-97 or SHELX-2014.[55] CCDC 834016 (**I**·2Br), 834017 (**II**·2Br), 834018 (**III**·2Br), 834019 (**IV**·2Br), 834020 (**V**·2Br), 834021 (*cis*-**2**·BrCl·3H$_2$O), 834022 (*trans*-**2**·0.75Br1.25Cl·4MeOH·2H$_2$O), 834023 (*cis*-**3**·2Br·2MeOH·3H$_2$O), 834024 (*cis*-**4**·2Br·2MeOH) and 834025 (*trans*-**4**·2Br·3MeOH) contain the supplementary crystallographic data for this paper.

Crystal data and structure refinement

I·2Br·2H$_2$O. M = 462.20, orthorhombic, space group $P2_12_12_1$, a = 8.1485(6), b = 14.5332(12), c = 15.4360(13) Å, V 1828.0(3) Å^3, Z 4, ρ_{calcd} 1.679 Mg m^{-3}, λ 0.48595 Å, μ 2.389 mm^{-1}, reflections collected 26 940, independent reflections 5197 [R(int) = 0.0587], max./min. transmission 1.00/0.80, data/restraints/parameters 5197/6/231. GoF 1.028. Final R indices [$I > 2\sigma(I)$] R_1 = 0.0281, wR_2 = 0.0618; R indices (all data) R_1 = 0.0329, wR_2 = 0.0635. Absolute structure parameter 0.13(2). Largest diff. peak and hole 0.984 and −0.424 e Å^{-3}.

II·2Br·C_3H_6O·H_2O. M = 516.28, triclinic, space group $P\bar{1}$ a = 9.2891(14), b = 11.4501(17), c = 11.666(2) Å, α = 104.754(2), β = 111.067(2), γ = 92.096(2)°, V 1108.4(3) Å^3, Z 2, ρ_{calcd} 1.547 Mg m^{-3}, λ 0.71073 Å, μ 3.679 mm^{-1}, reflections collected 10 429, independent reflections 5339 [R(int) = 0.032], max./min. transmission 1.00/0.84, data/restraints/parameters 5339/2/290. GoF 1.056. Final R indices [$I > 2\sigma(I)$]: R_1 = 0.0413, wR_2 = 0.0876; R indices (all data): R_1 = 0.0678, wR_2 = 0.0968. Largest diff. peak and hole 0.692 and −0.384 e Å^{-3}. The acetone solvent molecule was modelled as being disordered over two sets of sites with site occupancies of the two components refined to 0.668(5) and its complement.

III·2Br. M = 454.22, monoclinic, space group $P2_1/c$, a = 9.1040(4), b = 12.7208(6), c = 15.8340(10) Å, β = 101.216(5)°, V 1798.72(17) Å^3, Z 4, ρ_{calcd} 1.677 Mg m^{-3}, λ 0.71073 Å, μ 4.514 mm^{-1}, reflections collected 40 296, independent reflections 5046 [R(int) = 0.0301], max./min. transmission 1.21/0.74, data/restraints/parameters: 5046/0/217. GoF 1.012. Final R indices [$I > 2\sigma(I)$]: R_1 = 0.0307, wR_2 = 0.0808; R indices (all data): R_1 = 0.0439, wR_2 = 0.0837. Largest diff. peak and hole 1.640 and −0.796 e Å^{-3}.

IV·2Br·CH_3CH_2OH. M = 586.37, monoclinic, space group $P2_1/c$, a = 9.578(2), b = 22.0948(17), c = 13.560(2) Å, β = 90.175(17)°, V 2869.6(8) Å^3, Z 4, ρ_{calcd} 1.357 Mg m^{-3}, λ 0.71073 Å, μ 2.849 mm^{-1}, reflections collected 51 143, independent reflections 6588 [R(int) = 0.0550], max./min. transmission 1.00/0.51, data/restraints/parameters 6588/289/346. GoF 1.051. Final R indices [$I > 2\sigma(I)$]: R_1 = 0.0804, wR_2 = 0.2280; R indices (all data): R_1 = 0.1052, wR_2 = 0.2403. Largest diff. peak and hole 1.353 and −1.071 e Å^{-3}. One bromine atom was modelled as being disordered over two sites with occupancies refined to 0.806(3) and its complement. One solvent ethanol molecule is disordered about an inversion centre.

V·2Br. M = 554.33, monoclinic, space group $P2_1/n$, a = 12.6464(10), b = 13.5603(10), c = 13.6869(10) Å, β = 97.140(9)°, V 2329.0(3) Å^3, Z 4, ρ_{calcd} 1.581 Mg m^{-3}, λ 0.71073 Å, μ 3.503 mm^{-1}, reflections collected 64 688, independent reflections 7480 [R(int) = 0.0433], max./min. transmission 1.22/0.58, data/restraints/parameters 7480/0/308. GoF 0.983. Final R indices [$I > 2\sigma(I)$] R_1 = 0.0506, wR_2 = 0.1450; R indices (all data) R_1 = 0.0813, wR_2 = 0.1562. Largest diff. peak and hole 2.049 and −0.785 e Å^{-3}. The central two carbon atoms of the C_4 alkyl chain were modelled as being disordered over two sets of sites with occupancies set at 0.5 after trial refinement.

cis-**2**·BrCl·3H_2O. M = 1148.10, orthorhombic, space group $Pmc2_1$, a = 14.5133(5), b = 7.1167(2), c = 19.1502(5) Å, V 1977.96 (10) Å^3, Z 2, ρ_{calcd} 1.928 Mg m^{-3}, λ 0.71073 Å, μ 8.532 mm^{-1}, reflections collected 27 729, independent reflections 6523 [R(int) = 0.0789], max./min. transmission 1.00/0.38, data/restraints/parameters 6523/1/239. GoF 1.008. Final R indices [$I > 2\sigma(I)$]: R_1 = 0.0603, wR_2 = 0.1367; R indices (all data): R_1 = 0.0975, wR_2 = 0.1462. Absolute structure parameter 0.062(19). Largest diff. peak and hole 4.257 and −1.768 e Å^{-3}. The anionic sites were modelled as being occupied partially by chloride and bromide ions (for site (1)), or bromide and water (site (2)), or chlorine and water (site (3)) with occupancies set at 0.5 after trial refinement. Other peaks in the difference maps were modelled as being water molecules with occupancies set at either 1.0 or 0.5 after trial refinement and considerations of molecular interactions.

trans-**2**·0.75Br·1.25Cl·4MeOH·2H_2O. M = 1247.14, triclinic, space group $P\bar{1}$, a = 8.1215(5), b = 11.4030(10), c = 11.959(3) Å, α = 84.260(10), β = 82.030(10), γ = 78.157(7)°, V 1070.5(3) Å^3, Z 1, ρ_{calcd} 1.934 Mg m^{-3}, λ 71 073 Å, μ 7.678 mm^{-1}, reflections collected 49 142, independent reflections 10 859 [R(int) = 0.0374], max./min. transmission 1.00/0.40, data/restraints/parameters 10 859/3/275. GoF 1.017. Final R indices [$I > 2\sigma(I)$]: R_1 = 0.0227, wR_2 = 0.0403; R indices (all data): R_1 = 0.0320, wR_2 = 0.0416. Largest diff. peak and hole 4.395 and −1.041 e Å^{-3}. The halide site was modelled as being occupied part by bromine and part chlorine with the occupancies refining to Cl 0.624(2), Br 1–0.624(2).

cis-**3**·2Br·2MeOH·3H_2O. M = 1428.82, triclinic, space group $P\bar{1}$, a = 12.9166(3), b = 14.7735(3), c = 15.8256(3) Å, α = 114.049(2), β = 95.802(2), γ = 109.275(2)°, V 2504.04(9) Å^3, Z 2, ρ_{calcd} 1.895 Mg m^{-3}, λ 0.71073 Å, μ 7.504 mm^{-1}, reflections collected 67 453, independent reflections 29 220 [R(int) = 0.0347], max./min. transmission 0.203/0.064, data/restraints/parameters: 29 220/1/646. GoF 0.906. Final R indices [$I > 2\sigma(I)$]: R_1 = 0.0278, wR_2 = 0.0519; R indices (all data): R_1 = 0.0528, wR_2 = 0.0536. Largest diff. peak and hole 3.900 and −2.283 e Å^{-3}.

cis-**4**·2Br·2MeOH. M = 1402.82, orthorhombic, space group $C222_1$, a = 16.5234(2), b = 17.3329(2), c = 33.2686(3) Å, V 9528.08(18) Å^3, Z 8, ρ_{calcd} 1.956 Mg m^{-3}, λ 0.71073 Å, μ 7.882 mm^{-1}, reflections collected 109 454, independent reflections 23 678 [R(int) = 0.0623], max./min. transmission 1.00/0.43, data/restraints/parameters: 23 678/122/653. GoF 0.846. Final R indices [$I > 2\sigma(I)$]: R_1 = 0.0316, wR_2 = 0.0524; R indices (all data): R_1 = 0.0583, wR_2 = 0.0576. Absolute structure parameter: −0.043(4). Largest diff. peak and hole 2.859 and −1.526 e Å^{-3}. The atoms of one C_4 chain were modelled as being disordered over two sets of sites with occupancies refined to 0.708(3) and its complement. The solvent was modelled as two MeOH molecules, both disordered over two sets of sites with occupancies constrained, after trial refinement, to be the same as those of the disordered C_4 chain.

trans-**4**·2Br·3MeOH. M = 1434.86, monoclinic, space group $P2_1/n$, a = 12.6255(3), b = 27.8969(7), c = 15.7022(4) Å, β = 107.297(3)°, V 5280.4(2) Å^3, Z 4, ρ_{calcd} 1.805 Mg m^{-3}, λ 0.71073 Å, μ 7.115 mm^{-1}, reflections collected 49 310, independent reflections 9275 [R(int) = 0.0751], max./min. transmission 1.00/0.72, data/restraints/parameters 9275/537/703. GoF 1.223. Final R indices [$I > 2\sigma(I)$]: R_1 = 0.0954, wR_2 = 0.1958; R indices (all data): R_1 = 0.1504, wR_2 = 0.2095. Largest diff. peak and hole 2.623 and −1.672 e Å^{-3}. The bromide ions were modelled as being disordered over 5 sites with the sum of their occupancy factors constrained to be 2. The other remaining peaks were modelled as three methanol solvent molecules. The central atoms of the C_4 alkyl chains were modelled as being disordered over two sets of sites with occupancies set at 0.5 after trial refinement.

Measurement of lipophilicity

The octanol–water partition coefficients (log *P*) of *cis*-**1**·2Br, *cis*-**2**·2Br, *cis*-**3**·2Br and *cis*-**4**·2Br were determined using the shake-flask method.[43] Water (50 mL, milli-Q purification) and *n*-octanol (vacuum distilled) were shaken together using a laboratory shaker (Mistral Multi-Mixer) for 72 h to allow saturation of both phases. Stock solutions of the Au compounds (40 μM) were prepared in the aqueous phase and aliquots (1 mL) of each stock solution were then added to an equal volume of the *n*-octanol phase. The resultant solutions containing two phases were mixed for 1 h and following a short incubation at 37 °C were centrifuged (3000*g*, 5 min, Eppendorf Centrifuge 5415C) to separate the phases. The concentrations of the Au complexes in the organic and aqueous phases were determined using their UV absorbance (310 nm, 288 nm, 259 nm, and 315 nm, respectively for *cis*-**1**·2Br, *cis*-**2**·2Br, *cis*-**3**·2Br and *cis*-**4**·2Br). log *P* was defined as the logarithm of the ratio of the concentrations of each of the complexes in the organic and aqueous phases ($\log P = \log([Au_{org}]/[Au_{aq}])$; values reported are the means of three separate determinations).

Spectroscopy

Electronic absorption spectra were recorded on a Perkin Elmer Lambda 25 UV-Vis spectrometer, and luminescence excitation and emission spectra were recorded on a Varian Cary Eclipse Luminescence Spectrometer. The emission quantum yield (Φ) of *cis*-**3**·2Br was determined using standard procedures with respect to the quantum yield of a reference (Φ_R) according to eqn (1):[42,56]

$$\Phi = \Phi_R \frac{I}{I_R} \frac{n^2}{{n_R}^2} \quad (1)$$

where I is the gradient of the standard curve of absorbance *vs.* integrated emission intensity for *cis*-**3**·2Br, I_R is the gradient of the standard curve of absorbance *vs.* integrated emission intensity for the reference solution, n is the refractive index of the solution and the subscript R refers to the reference fluorophore of known quantum yield. The reference used was quinine sulfate (Alfa Aesar, 98%), dissolved in 0.1 M H_2SO_4, and having $\Phi_R = 0.577$ (T = 22 °C).[41,42] Measurements were made using two excitation wavelengths, λ_{ex} = 288 and 345 nm.

Cell culture

Human cervical cancer (HeLa, ATCC) cells were cultured at 37 °C under humidified 95% air/5% CO_2 in Dulbecco's modified Eagle's medium (DMEM) without phenol red, containing Earle's balanced salt solution and supplemented with 2 mM GlutaMAX, penicillin (100 U mL^{-1}), streptomycin (100 mg mL^{-1}) and 10% heat inactivated foetal calf serum (FCS). MDA-MB-231 human breast adenocarcinoma cells (MDA, ATCC, kindly donated by Prof. A. Dharmarajan, School of Anatomy and Human Biology, University of Western Australia) were cultured at 37 °C under humidified 95% air/5% CO_2 in RPMI 1640 GlutaMAX (Gibco/Invitrogen), supplemented with 10% foetal bovine serum, penicillin G sodium (10^3 units per mL), streptomycin sulfate (10 mg mL^{-1}) and amphotericin B (25 μg mL^{-1}). Both cell lines were passaged every 3–5 days.

Cell proliferation/viability

HeLa cells grown in 96 well plates were incubated for 24 h in 200 μL of their growth medium containing increasing concentrations of *cis*-**1**·2Br, *trans*-**1**·2Br, *cis*-**3**·2Br or *trans*-**3**·2Br. Cell viability was determined using a cell titer assay following the manufacturer's instructions (Promega, G3580). The assay was performed by adding 7 μL of the CellTiter 96® Aqueous One Solution Reagent (MTS assay) directly to the culture wells, incubating for 1 h, and then recording the absorbance at 490 nm in a BMG Labtech Fluostar Optima plate reader. The data are expressed as percent of cells grown in the absence of any Au complexes. Data are means ± SD of three independent experiments.

Luminescence microscopy of live MDA cells

MDA cells were grown in a 2.5 mL culture chamber for 24 h in RPMI 1640 phenol red free medium (Gibco/Invitrogen) with no antibiotics or foetal calf serum. A stock solution of *cis*-**3**·2Br (1 mg in 5 mL DMSO) was prepared, and immediately before use, the solution was centrifuged (3000*g*, 1 min). Immediately before imaging, the medium was removed from the cells and the cells were washed twice with PBS (500 μL), before the addition of fresh medium (1 mL) and 50 μL of the above *cis*-**3**·2Br solution. The cells were viewed on a Nikon Eclipse TI inverted microscope using UV illumination (BP filter 340–380 nm), and images collected on a Coolsnap EZ digital camera (Roper Scientific) every 30 s for a period of 6 h (emission LP 425 nm). NIS Elements AR software was used to convert the images in Quicktime movie format. Final *cis*-**3**·2Br concentration was determined using the extinction coefficient for absorbance at 290 nm (ε = 22 000, determined using a 2.12×10^{-5} M solution of *cis*-**3**·2Br in DMSO), to give final concentration of 0.55 mM stock, and 26.2 μM *cis*-**3**·2Br exposed to the cells.

Acknowledgements

We thank the Australian Research Council for financial support (DP0452327 to S. J. B.-P. and M. V. B. and DP0986318 to S. J. B.-P. and A. F.) and an Australian Postgraduate Award (to L. E. W.). A. F. is a National Health and Medical Research Council Senior Research Fellow. We also thank Professor Luis Filgeuira, for donation of MDA cells and access to some laboratory facilities. We acknowledge the Centre of Microscopy, Characterisation and Analysis, The University of Western Australia (a facility funded by The University of Western Australia, the Australian Government and the State Government of Western Australia) for providing access to facilities, and for scientific and technical assistance. Use of the ChemMatCARS Sector 15 at the Advanced Photon Source, for **I**·2Br·2H_2O, was supported by the Australian Synchrotron Research Program, which is funded by the Commonwealth of Australia under the Major National Research Facilities Program.

Notes and references

1 P. Cabildo, D. Sanz, R. M. Claramunt, S. A. Bourne, I. Alkorta and J. Elguero, *Tetrahedron*, 1999, **55**, 2327–2340.
2 I. Bitter, Z. Török, V. Csokai, A. Grün, B. Balázs, G. Tóth, G. M. Keserú, Z. Kovári and M. Czugler, *Eur. J. Org. Chem.*, 2001, 2861–2868.
3 M. V. Baker, M. J. Bosnich, D. H. Brown, L. T. Byrne, V. J. Hesler, B. W. Skelton, A. H. White and C. C. Williams, *J. Org. Chem.*, 2004, **69**, 7640–7652.
4 M. V. Baker, D. H. Brown, C. H. Heath, B. W. Skelton, A. H. White and C. C. Williams, *J. Org. Chem.*, 2008, **73**, 9340–9352.
5 M. V. Baker and D. H. Brown, *Mini-Rev. Org. Chem.*, 2006, **3**, 333–354.
6 V. J. Hesler, B. W. Skelton, A. H. White, D. H. Brown and M. V. Baker, *J. Inclusion Phenom. Macrocyclic Chem.*, 2015, **82**, 53–69.
7 E. Alcalde, I. Dinarès and N. Mesquida, *Top. Heterocycl. Chem.*, 2010, **24**, 267–300.
8 S. Ramos, E. Alcalde, J. Fraser Stoddart, A. J. P. White, D. J. Williams and L. Perez-Garcia, *New J. Chem.*, 2009, **33**, 300–317.
9 E. Alcalde, N. Mesquida and L. Perez-Garcia, *Eur. J. Org. Chem.*, 2006, 3988–3996.
10 E. Alcalde, N. Mesquida, M. Vilaseca, C. Alvarez-Rua and S. Garcia-Granda, *Supramol. Chem.*, 2007, **19**, 501–509.
11 M. V. Baker, B. W. Skelton, A. H. White and C. C. Williams, *J. Chem. Soc., Dalton Trans.*, 2001, 111–120.
12 M. V. Baker, B. W. Skelton, A. H. White and C. C. Williams, *Organometallics*, 2002, **21**, 2674–2678.
13 P. J. Barnard, M. V. Baker, S. J. Berners-Price, B. W. Skelton and A. H. White, *Dalton Trans.*, 2004, 1034–1047.
14 E. Alcalde, R. M. Ceder, C. Lopez, N. Mesquida, G. Muller and S. Rodriguez, *Dalton Trans.*, 2007, 2696–2706.
15 S. Durmus, J. C. Garrison, M. J. Panzner, C. A. Tessier and W. J. Youngs, *Tetrahedron*, 2004, **61**, 97–101.
16 J. C. Garrison, R. S. Simons, W. G. Kofron, C. A. Tessier and W. J. Youngs, *Chem. Commun.*, 2001, 1780–1781.
17 J. C. Garrison, R. S. Simons, J. M. Talley, C. Wesdemiotis, C. A. Tessier and W. J. Youngs, *Organometallics*, 2001, **20**, 1276–1278.
18 J. C. Garrison, R. S. Simons, C. A. Tessier and W. J. Youngs, *J. Organomet. Chem.*, 2003, **673**, 1–4.
19 A. Melaiye, Z. Sun, K. Hindi, A. Milsted, D. Ely, D. H. Reneker, C. A. Tessier and W. J. Youngs, *J. Am. Chem. Soc.*, 2005, **127**, 2285–2291.
20 R. S. Simons, J. C. Garrison, W. G. Kofron, C. A. Tessier and W. J. Youngs, *Tetrahedron Lett.*, 2002, **43**, 3423–3425.
21 V. J. Hesler, B. W. Skelton, A. H. White, D. H. Brown and M. V. Baker, *J. Inclusion Phenom. Macrocyclic Chem.*, 2015, **82**, 71–78.
22 W. Liu and R. Gust, *Chem. Soc. Rev.*, 2013, **42**, 755–773.
23 L. Oehninger, R. Rubbiani and I. Ott, *Dalton Trans.*, 2013, **42**, 3269–3284.
24 J. L. Hickey, R. A. Ruhayel, P. J. Barnard, M. V. Baker, S. J. Berners-Price and A. Filipovska, *J. Am. Chem. Soc.*, 2008, **130**, 12570–12571.
25 O. Rackham, A.-M. J. Shearwood, E. Thyer, E. McNamara, S. M. K. Davies, B. A. Callus, A. Miranda-Vizuete, S. J. Berners-Price, Q. Cheng, E. S. J. Arner and A. Filipovska, *Free Radicals Biol. Med.*, 2010, **50**, 689–699.
26 P. J. Barnard, M. V. Baker, S. J. Berners-Price and D. A. Day, *J. Inorg. Biochem.*, 2004, **98**, 1642–1647.
27 P. J. Barnard, L. E. Wedlock, M. V. Baker, S. J. Berners-Price, D. A. Joyce, B. W. Skelton and J. H. Steer, *Angew. Chem., Int. Ed.*, 2006, **45**, 5966–5970.
28 H. Schmidbaur, *Gold Bull.*, 1990, **23**, 11–21.
29 H. Schmidbaur, *Gold Bull.*, 2000, **33**, 3–10.
30 H. Schmidbaur and A. Schier, *Chem. Soc. Rev.*, 2008, **37**, 1931–1951.
31 H. Schmidbaur, *Chem. Soc. Rev.*, 1995, **24**, 391–400.
32 P. Pyykko, *Chem. Soc. Rev.*, 2008, **37**, 1967–1997.
33 V. W.-W. Yam and E. C.-C. Cheng, *Chem. Soc. Rev.*, 2008, **37**, 1806–1813.
34 V. W.-W. Yam and E. C.-C. Cheng, *Top. Curr. Chem.*, 2007, **281**, 269–309.
35 A. Vogler and H. Kunkely, *Coord. Chem. Rev.*, 2001, **219–221**, 489–507.
36 M. Ferrer, A. Gutiérrez, L. Rodríguez, O. Rossell, J. C. Lima, M. Font-Bardia and X. Solans, *Eur. J. Inorg. Chem.*, 2008, 2899–2909.
37 L. Rodríguez, M. Ferrer, R. Crehuet, J. Anglada and J. C. Lima, *Inorg. Chem.*, 2012, **51**, 7636–7641.
38 L. E. Wedlock, J. B. Aitken, S. J. Berners-Price and P. J. Barnard, *Dalton Trans.*, 2013, **42**, 1259–1266.
39 M. V. Baker, D. H. Brown, R. A. Haque, B. W. Skelton and A. H. White, *Dalton Trans.*, 2004, 3756–3764.
40 M. V. Baker, D. H. Brown, R. A. Haque, P. V. Simpson, B. W. Skelton, A. H. White and C. C. Williams, *Organometallics*, 2009, **28**, 3793–3803.
41 J. W. Eastman, *Photochem. Photobiol.*, 1967, **6**, 55–72.
42 F. R. Lakowicz, *Principles of Fluorescence Spectroscopy*, Kluwer Academic/Plenum Publishers, New York, 2nd edn, 1999.
43 A. Albert, *The Physiochemical Basis of Therapy*, Chapman and Hall, London, 1979.
44 D. Parker, *Aust. J. Chem.*, 2011, **64**, 239–243.
45 J. Lemke, A. Pinto, P. Niehoff, V. Vasylyeva and N. Metzler-Nolte, *Dalton Trans.*, 2009, 7063–7070.
46 S. D. Köster, H. Alborzinia, S. Can, I. Kitanovic, S. Wölfl, R. Rubbiani, I. Ott, P. Riesterer, A. Prokop, K. Merza and N. Metzler-Nolte, *Chem. Sci.*, 2012, **3**, 2062–2072.
47 H. E. Gottlieb, V. Kotlyar and A. Nudelman, *J. Org. Chem.*, 1997, **62**, 7512–7515.
48 D. D. Perrin, W. L. F. Armarego and D. R. Perrin, *Purification of Laboratory Chemicals*, Pergamon Press Ltd, 2nd edn, 1980.
49 E. F. M. Stephenson, *Org. Synth.*, 1954, **34**, 100–102.
50 L. P. Wu, Y. Yamagiwa, T. Kuroda-Sowa, T. Kamikawa and M. Munakata, *Inorg. Chim. Acta*, 1997, **256**, 155–159.

51 M. Luo, S. Guo, C. Zhou and R. Xie, *Heterocycles*, 1995, **41**, 1421–1424.
52 J.-F. Ma, J. Yang, G.-L. Zheng, L. Li and J.-F. Liu, *Inorg. Chem.*, 2003, **42**, 7531–7534.
53 Z. Shi and R. P. Thummel, *J. Org. Chem.*, 1995, **60**, 5935–5945.
54 M.-C. Brandys, M. C. Jennings and R. J. Puddephatt, *Dalton Trans.*, 2000, 4601–4606.
55 G. M. Sheldrick, *Acta Crystallogr., Sect. C: Cryst. Struct. Commun.*, 2015, **71**, 3–8.
56 C. A. Parker, *Photoluminescence of Solutions*, Elsevier Publishing Company, Amsterdam, 1st edn, 1968.